rRNA intermediates coordinate the multilayered nucleolar phase transition in *C. elegans*

Demin Xu[1‡], Xiangyang Chen[1‡], Yan Kuang[1], Minjie Hong[1], Ting Xu[1], Ke Wang[1], Chuanhai Fu[1], Ke Ruan[1], Chengming Zhu[1*], Xuezhu Feng[1*] and Shouhong Guang[1,2*]

[1]Department of Obstetrics and Gynecology, The First Affiliated Hospital of USTC, The USTC RNA Institute, Ministry of Education Key Laboratory for Membraneless Organelles & Cellular Dynamics, School of Life Sciences, Division of Life Sciences and Medicine, Biomedical Sciences and Health Laboratory of Anhui Province, University of Science and Technology of China, Hefei, Anhui 230027, China

[2]CAS Center for Excellence in Molecular Cell Science, Chinese Academy of Sciences, Hefei, Anhui 230027, P.R. China

[‡]These authors contributed equally to this work.

[*]Correspondence should be addressed to zcm916@ustc.edu.cn, fengxz@ustc.edu.cn, sguang@ustc.edu.cn

Abstract

The nucleolus is the most prominent membraneless organelle within the nucleus and plays essential roles in rRNA transcription and processing and ribosome assembly. How the structure of the nucleolus is maintained and regulated is poorly understood. Here, we identified two types of nucleoli in *C. elegans*. Type I nucleoli are spherical, and rRNA transcription and processing factors are evenly distributed throughout the nucleolus. In type II nucleoli, rRNA transcription and processing factors exclusively accumulate in the periphery rim, which is named the nucleolar ring. The hollow vacuole inside the nucleolar ring contains proteins that usually localize in the nucleoplasm but are capable of exchanging contents across the ring. The high-order structure of the nucleolus is dynamically regulated in *C. elegans*. Faithful rRNA processing is important to maintain the spherical structure of the nucleoli. The depletion of a class of rRNA processing factors, for example, class I ribosomal proteins of the large subunit (RPL), which are involved in $27SA_2$ rRNA processing, reshaped spherical nucleoli to a ring-shaped nucleolar structure. The inhibition of RNAP I transcription and depletion of two conserved nucleolar factors, nucleolin and fibrillarin, prohibits the formation of the nucleolar ring. We concluded that the integrity of nucleoli is highly dependent on rRNA processing and maturation, which may provide a mechanism to coordinate structure maintenance and gene expression.

Keywords: nucleolus, vacuole, ring, reshaping, rRNA, RNAP I, phase transition

Introduction

The nucleolus is the most prominent membraneless organelle within the nucleus and forms around tandem arrays of ribosomal gene repeats, termed nucleolar organizer regions (1). The nucleolar proteome identified more than 1000 different proteins, most of which are involved in ribosome biogenesis, including rRNA transcription and processing and ribosome assembly (2, 3). An increasing number of studies suggest that the nucleolus is a multilayered biomolecular condensate that assembles via liquid–liquid phase separation (LLPS) (4-7). In vitro reconstitution studies suggested that the key nucleolar proteins, fibrillarin and nucleophosmin, can undergo LLPS (4). In *X. laevis* germinal vesicles, nucleoli exhibit liquid-like behavior and spontaneously coalesce and round up upon contact (5). In addition, it was suggested that the organization of nucleolar subcompartments arises through multiphase liquid immiscibility, which is driven by the differential surface tension of substructures (4, 8).

The nucleoli of mammalian cells display three internal phase-separated subcompartments, the fibrillar center (FC), the dense fibrillar component (DFC), and the granular component (GC) (7). Typically, the FC is surrounded by a shell of DFC; both are enclosed in the GC. Recent work has suggested that *C. elegans* nucleoli also contain two phase-separated subcompartments, GC and FC (9). In addition, there is a highly conserved central region, called the nucleolar cavity or vacuole, present in the nucleoli of various plants and animals, which was first observed in the 19th century (Fig. 1A) (9-13). Similar vacuoles have been observed in mammalian cells, such as in MCF-7, COS-7 and Hep-2 cells (14).

Although nucleolar vacuoles have been discovered for more than a hundred years, their regulatory mechanism, composition and function remain unclear. In *soybean,* different types of cellular stresses and environmental stimuli, for example, cold-warm treatment, led to the formation of nucleolar vacuoles (15, 16). Similarly, nucleolar vacuoles were formed in heat and chilling stress-treated *Arabidopsis thaliana* (17) and 5-fluoro-uracil-treated *Jerusalem artichoke tubers* (13). Drugs inhibiting rRNA

synthesis, including actinomycin D, 5-fluoro-uracil and 2-thio-uracil, could impede vacuole formation in *tobacco callus* and *Zea mays* cells (18, 19). The vacuoles may contain ribonucleoprotein (RNP) complexes because both small nuclear RNAs (snRNAs) and small nucleolar RNAs (snoRNAs) have been detected (20, 21). It was postulated that nucleolar vacuoles may engage in mRNA surveillance and export, transport of nucleolar substances and temporary storage of certain materials (12, 13, 15, 22). In addition, larger vacuoles may be linked to higher nucleolar activity (15).

Here, we investigated the nucleolar structure of *C. elegans* and identified two types of nucleoli: spherical and ring-shaped nucleoli. We conducted candidate-based RNAi screening and identified a distinct class of RPLs, the knockdown of which reshaped spherical nucleoli to ring-shaped nucleoli and therefore were named class I RPLs. Interestingly, the ring-shaped nucleoli exhibited reentrant phase transition behavior by monotonically increasing $27SA_2$ pre-rRNAs. Through circularized reverse-transcription PCR (cRT-PCR), we detected abnormal accumulation of $27SA_2$ rRNAs upon the depletion of class I RPLs. The ring-shaped nucleoli had a subcompartment termed the nucleolar vacuole, which contains proteins usually localized in the nucleoplasm. NUCL-1 and FIB-1, two highly conserved nucleolar proteins with internal disordered sequences, were required for the formation of the nucleolar ring. The work suggested that the structure of the nucleolus is highly coordinated with rRNA processing and maturation.

Results

Identification of two-shaped nucleoli in *C. elegans*.

During the culture of *C. elegans*, we frequently observed hollow nucleoli with rim and vacuole structures by differential interference contrast (DIC) microscopy (Fig. S1A). To further explore the nucleolar structure, we generated an RRP-8::GFP transgene to label the nucleoli (23). The nucleoli were visualized by DIC and fluorescence microscopy. We identified two types of nucleoli in *C. elegans*. In type I

nucleoli, RRP-8::GFP likely evenly occupied the entire nucleoli, and the nucleoli were spherical under a DIC microscope (Fig. 1B). The type II nucleoli were convex in the periphery and concave in the center under DIC (Fig. 1B). RRP-8::GFP was strongly enriched in the periphery of the nucleoli and colocalized with the convex region but did not accumulate in the center. Therefore, we named the convex part the nucleolar ring and the concave part the nucleolar vacuole (Fig. 1A). Both types of nucleoli existed in different tissues (Figs. 1B-C). In epidermal cells and gonadal cells, the nucleoli were mainly spheres, and in intestinal cells, the nucleoli were mainly ring-shaped. The nucleolar structure in the germline is reshaped dynamically during development. The percentage of ring-shaped nucleoli in the germline was increased during germline maturity in young gravid adults and reduced in aged animals, suggesting reshaping processes between spherical and ring-shaped nucleoli (Figs. 1D-E).

Class I *rpl* genes are required to maintain nucleolar structural integrity.

To explore the mechanism of nucleolar structure formation, we conducted candidate-based RNAi screening to search for factors that are required to maintain the two-shaped nucleoli. We selected 110 genes that were involved in rRNA processing and ribosome assembly and knocked down these genes by feeding RNAi (Fig. 2A, Table S1). Then, we visualized the nucleolar morphology and localization of RRP-8::GFP. Of 48 *rpl* genes, knocking down a group of 19 *rpl* genes significantly increased the proportion of ring-shaped nucleoli (Figs. 2B-D, S1B-E). We divided the 48 *rpl* genes into two classes according to whether knocking down the gene could promote the formation of ring-shaped nucleoli (Fig. 2E). Knocking down class I *rpl* genes significantly increased the size of nucleoli and nucleolar vacuoles (Figs. 2F-H and S1F) and slightly increased the size of nucleolar rings (Figs. 2I-K).

The nucleolus is likely formed by LLPS, which is modulated by environmental temperature. Many disordered proteins and/or nucleic acids undergo LLPS either upon cooling or heating (24-27). Heat and chilling stress have been shown to induce the formation of nucleolar vacuoles in *Arabidopsis thaliana* (17). Previously, we showed

that cold stress induced the production of risiRNA and the accumulation of two nucleoplasmic proteins, NRDE-2 and NRDE-3, in the nucleoli in *C. elegans* (23, 28, 29). We then investigated the effect of cold stress on nucleolare reshaping. In wild-type animals, the ring-shaped nucleoli were suppressed by 4°C cold stress and reverted when shifting back to 20°C (Figs. S2A-B). Similarly, the formation of *rpl-14 knockdown*-induced ring-shaped nucleoli was strongly prohibited by cold stress, and this inhibition was released after transferring the worms to 20°C for 24 hours (Figs. S2C-D).

rRNA transcription and processing machinery accumulate in the nucleolar ring.

The factors involved in rRNA transcription and processing and ribosome assembly are largely evenly dispersed in the spherical nucleolus (23, 30). To test whether nucleolar reshaping could transform the localization of other rRNA transcription and processing factors in addition to RRP-8, we generated transgenes of a number of nucleolus-localized proteins and examined their localization upon knocking down *rpl-14* by RNAi. FIB-1 is a conserved fibrillarin involved in nucleologenesis and is usually used as a nucleolar marker (31, 32). RBD-1 is an ortholog of human RBM19, which is required for 90S pre-ribosome maturation (33). Both FIB-1 and RBD-1 occupied the entire spherical nucleolus in wild-type animals and accumulated in the nucleolar ring upon RNAi *rpl-14* (Figs. 3A-B). RPOA-1, RPOA-2 and RPAC-19 are subunits of the RNA polymerase I complex and are dispersed in the spherical nucleolus and accumulated in the nucleolar ring upon *rpl-14* RNAi (Figs. 3C-D, S3A). DAO-5, an rRNA transcription factor, also translocated to the nucleolar ring upon *rpl-14* RNAi (Fig. S3B). Consistently, DAO-5 has been previously reported to localize in the nucleolar ring in intestine cells in wild-type animals (31). rRNA processing proteins, such as RPL-7 and T06E6.1, were enriched in the nucleolar ring upon *rpl-14* RNAi (Figs. S3C-D). These results are summarized in Fig. 3E and imply that the nucleolar ring may still be capable of conducting rRNA transcription and processing.

We investigated the localization of nucleic acids after spherical to ring-shaped nucleolar reshaping. Both DAPI staining and GFP::HIS-71 (HIS-3.3) transgene

169 indicated that DNA was enriched in the nucleoplasm in both spherical and ring-shaped
170 nucleoli but likely depleted from the nucleolar vacuole (Figs. 3F-G, S3E-F). An RNA-
171 specific dye, SYTO RNASelect, is usually used to stain abundant rRNAs. In control
172 animals, RNA was evenly distributed in the whole spherical nucleoli (Fig. S3G-H).
173 However, knocking down *rpl-14* enriched RNAs in the nucleolar ring but depleted them
174 from nucleolar vacuoles (17).
175
176 The phase separation ability of nucleoli is essential for their function (7). We
177 performed a FRAP assay to investigate whether nucleolar reshaping alters the mobility
178 of rRNA transcription and processing machinery by comparing the mobility of RRP-8,
179 RPOA-1 and RPOA-2 in spherical and ring-shaped nucleoli. All three proteins did not
180 alter their mobility after bleaching in the sperical nucleoli and the nucleolar ring (Figs.
181 3H-J). These data suggested that nucleolar reshaping may not change the mobility of
182 the components for rRNA transcription and processing and implied that the nucleolar
183 ring is still able to conduct the reactions for rRNA transcription, processing and
184 ribosome assembly.
185
186 **Nucleoplasmic proteins accumulate in nucleolar vacuoles.**
187 To investigate the composition of nucleolar vacuoles, we generated a number of
188 fluorescence-labeled transgenes that usually accumulate in the nucleoplasm and are
189 involved in pre-mRNA transcription and processing. We visualized their subcellular
190 localization with and without *rpl-14* RNAi.
191
192 AMA-1 is the core subunit of RNA polymerase II. TAF-12 is a subunit of the
193 transcription factor TFIID complex. GTF-2H2C is a subunit of the transcription factor
194 TFIIH holo complex. AMA-1, TAF-12 and GTF-2H2C all accumulated in the nucleolar
195 vacuole in wild-type animals (Fig. S4A) and upon *rpl-14* RNAi (Figs. 4A-C). MTR-4
196 and EMB-4 are two pre-mRNA processing factors and are involved in nuclear RNAi
197 (34, 35). NRDE-2 and NRDE-3 are two proteins required for nuclear and nucleolar
198 RNAi (28, 34, 36, 37). We observed vacuolar localization of these factors in both wild-

type N2-background animals (Figs. S4B-D) and *rpl-14* RNAi animals (Figs. S4E-I). EXOS-2 is a subunit of the RNA exosome and accumulates in the nucleoplasm, nucleolar ring and vacuole (Fig. S4D). We summarized these data in Fig. 4D.

The nucleolus is physically separated from the nucleoplasm but rapidly exchanges its content with the surrounding nucleoplasm (7). To test whether the nucleolar ring could block the composition exchange between the nucleolar vacuole and nucleoplasm, we performed FRAP assays of GFP::NRDE-2 and GFP::MTR-4 in the nucleoplasm and nucleolar vacuole. Thirty seconds after bleaching, the GFP::NRDE-2 and GFP::MTR-4 fluorescence intensity in the nucleolar vacuole recovered to approximately 60% of the control fluorescent intensity (Fig. 4E). GFP::NRDE-2 exhibited similar mobility by FRAP in the nucleoplasm before and after *rpl-14* RNAi and in the nucleolar vacuole (Fig. 4F). However, GFP::NRDE-2 fluorescence did not recover when the whole nucleus was bleached (Fig. S4J). These data suggested frequent protein exchange between the nucleoplasm and the nucleolar vacuole.

NXF-1 is an mRNA export factor (38). NXF-1 was highly enriched in the nucleolar vacuole in wild-type N2 animals and upon *rpl-14* RNAi in epidermal cells (Figs. S5A-C). Interestingly, NXF-1 revealed a development-related vacuolar enhancement in germline cells in wild-type animals (Figs. S5D-E). In *A. thaliana,* similar vacuolar localization was reported for mRNA splicing proteins, U1 snRNP-specific proteins and exon–exon junction complex proteins (39). Taken together, these data implied that the nucleolar vacuole is capable of conducting mRNA biogenesis and regulation.

Class I *rpl* genes are required for 27SA$_2$ rRNA processing.

RPLs are proteins of the 60S ribosome subunit that are involved in ribosome assembly as well as pre-rRNA processing (40). To investigate the mechanism of nucleolar reshaping by class I RPL proteins, we adopted a circularized reverse-transcription PCR (cRT-PCR) method to analyze rRNA intermediates upon knocking down *rpl* genes (Fig. 5A) (41, 42). To validate the method, we performed cRT-PCR

followed by sequencing the ends of mature 5.8S, 18S and 26S rRNAs (Fig. S6A-C). The results were largely consistent with sequences annotated by Wormbase (29, 43).

Then, we assayed 26S rRNA intermediates by primer sets targeting the IVS II region upon knocking down *rpl* genes (Fig. 5B) and detected two major bands by the cRT-PCR method (Fig. 5B). We cloned and sequenced the 5' and 3' ends of these two bands and confirmed $27SA_2$ and 27SB pre-rRNAs (Fig. 5C). Strikingly, knocking down class I *rpl* but not class II *rpl* consistently led to the accumulation of $27SA_2$ pre-rRNA intermediates (Figs. 5D-E), implying that $27SA_2$ pre-rRNA or its processing may be involved in the formation of ring-shaped nucleoli.

RPS proteins are 40S ribosome subunits. We examined 18S rRNA intermediates after knocking down two *rps* genes, *rps-1* and *rps-5*. A number of additional 18S precursors were identified by cRT-PCR followed by sequencing (Figs. S7A-J). According to the identified 18S and 26S rRNA intermediates, a schematic diagram was drawn to reveal pre-rRNA processing steps (Fig. S8A).

To further confirm that $27SA_2$ rRNA is involved in the formation of ring-shaped nucleoli, we knocked down 26 predicted 60S rRNA processing factors by RNAi (Table S2). Feeding RNAi targeting 8 genes led to the formation of ring-shaped nucleoli (Figs. S8B-C). Most of the eight genes have been reported to be involved in 27SA and 27SB pre-rRNA processing (44, 45). Consistently, $27SA_2$ rRNAs accumulated upon knocking down these genes, as assayed by cRT-PCR (Figs. S7D-E).

Taken together, these data suggested that rRNA processing steps or intermediates were involved in the maintenance of nucleolar structure.

FIB-1 and NUCL-1 are required for nucleolar reshaping.

Intrinsically disordered regions (IDRs) are likely one of the driving forces of LLPS and have been identified in many phase-separated proteins (4, 46, 47). In addition, the

GAR/RGG domain is an RNA binding segment that is frequently present in proteins capable of conducting LLPS (46-48). To further understand the mechanism of nucleolar reshaping, we searched the *C. elegans* genome for proteins that have both IDR and GAR/RGG domains and are predicted to localize in the nucleoli. We identified 8 proteins (Figs. 6A, S9A), among which knocking down *nucl-1* and *fib-1* strongly blocked the formation of *rpl-14*-induced ring-shaped nucleoli (Figs. 6B-C).

FIB-1 is a highly conserved nucleolar protein with a GAR/RGG domain and methyltransferase domain that is involved in the methylation of pre-RNAs and nucleologenesis by LLPS (4, 22). NUCL-1 encodes an evolutionarily conserved protein exhibiting extensive homology to yeast and human nucleolin (9). The N-terminal domain of NUCL-1 is a long IDR containing a GAR/RGG domain, a methyltransferase domain, and an acidic stretch (Fig. 6A). The C-terminus of NUCL-1 harbors an RRM domain. Previous studies have shown that nucleolin associates with nascent pre-rRNA (49). Nucleolin in mammalian cells displays high mobility and is likely involved in phase separation (50). To confirm that NUCL-1 is required for the formation of ring-shaped nucleoli, we generated two additional deletion alleles of NUCL-1 by CRISPR/Cas9 technology (Fig. S9B). Both alleles inhibited the formation of *rpl-14 knockdown*-induced ring-shaped nucleoli (Figs. S9C-D). The FRAP assay revealed that the spherical nucleoli exhibited similar mobility in *nucl-1;rpl-14* animals to those in control animals (Fig. 6D). cRT-PCR showed that FIB-1 and NUCL-1 did not block the accumulation of $27SA_2$ (Figs. 6E-F, S9E-F), which suggested that FIB-1 and NUCL-1 functioned downstream of $27SA_2$ accumulation.

In vitro experiments showed that monotonically increasing RNA concentration could induce the formation of dynamic hollow condensates at high RNA-to-RNP ratios, but a disappearance at further higher RNA-to-RNP ratios, through multivalent heterotypic interactions that mediate a reentrant phase transition of RNPs containing arginine-rich IDR (51-53). To test whether nucleoli can undergo a reentrant phase transition in vivo during the nucleolar reshaping process, we conducated a time course

of *rpl-14* RNAi and examined the nucleolar morphology. Surprisingly, knocking down *rpl-14* induced the formation of nucleolar rings during the early phase of RNAi, yet the ring-shaped nucleoli gradually disappeared after long-term *rpl-14* RNAi (Figs. 6G-H), suggesting an in vivo reentrant phase transition of the nucleoli (51). Consistently, $27SA_2$ rRNA monotonically increased during the time course of *rpl-14* RNAi (Figs. 6I, S9G).

Taken together, we speculate that NUCL-1 and FIB-1 participate in the regulation of nucleolar morphology through phase transition.

Inhibiting rRNA transcription prohibits nucleolar reshaping.

Nucleoli undergo dramatic changes when encountering cellular stresses and environmental stimuli. A previous study revealed that actinomycin D, which inhibits RNA polymerase I activity, could impede vacuole formation (18, 19).

To investigate the mechanism of the spherical-to-ring transition, we knocked down *rpl-14* by RNAi in the presence of actinomycin D. A 10 μg/ml actinomycin D treatment did not noticeably change the localization of RRP-8 or the size of nucleoli in wild-type N2 animals (Fig. 7A) but inhibited the formation of *rpl-14 knockdown*-induced nucleolar rings (Figs. 7B-C). At a higher concentration of actinomycin D (20 μg/ml), the *rpl-14*-induced nucleolar ring was completely inhibited, and RRP-8 likely accumulated as a nucleolar cap structure (54). Consistently, actinomycin D treatment inhibited the accumulation of *rpl-14*-induced $27SA_2$ rRNA intermediates by cRT-PCR assay (Figs. 7D).

Discussion

The nucleolus is the most important membraneless organelle in the cell. Here, we observed two types of nucleoli, spherical and ring-shaped. The knockdown of class I RPL proteins, which are involved in $27SA_2$ rRNA processing, reshaped the spherical nucleoli to ring-shaped nucleoli (Fig. 7E). In ring-shaped nucleoli, rRNA transcription

and processing factors accumulate in the nucleolar ring, and a large number of nucleoplasmic proteins accumulate in the nucleolar vacuole. The inhibition of RNAP I transcription by actinomycin D and depletion of two conserved nucleolar factors, nucleolin and fibrillarin, prohibit the formation of nucleolar rings.

Regulation of nucleolar morphology by 27SA$_2$ rRNA.

The formation of multiphasic nucleolar structures may be due to the interaction of nucleolar proteins and rRNAs (4). Here, we found that the factors inhibiting the formation of ring-shaped nucleoli are all involved in 27SA$_2$ rRNA processing, suggesting that the 27SA$_2$ rRNA intermediates may play an important role in nucleolar morphology regulation. Similar to the ring-shaped nucleolus, [RGRGG]$_5$ polypeptides and cellular RNAs can form hollow condensates in vitro (53). An in vitro experiment indicated that monotonically increasing the RNA concentration in mixtures of synthetic peptides containing multivalent arginine-rich linear motifs can induce dynamic droplet substructure formation and disapperance (51). Poly-L-lysine and single-stranded oligodeoxynucleotide droplets were shown to undergo repeated cycles of vacuole nucleation, growth and expulsion in applied electric fields (55). The RNA binding protein TDP-43 can also form hollow condensates in cells by LLPS if its RNA-binding capacity is disrupted (56). Here, we found that in *C. elegans*, the nucleoli exhibited similar reentrant phase transition behavior upon *rpl-14* RNAi, which can be inhibited by knocking down two conserved RNA binding proteins, NUCL-1 and FIB-1, both of which contain arginine-rich IDR. Further experiments are required to test the causal relationship between 27SA$_2$ rRNAs and the formation of NUCL-1 or FIB-1 hollow condensates. Additionally, rRNA processing and maturation steps are highly conserved among eukaryotes. It will be very interesting to test whether 27SA$_2$ rRNAs are involved in the maintenance of the hollow structure in plants or DFC/GC regions in mammalian cells.

It is unclear how and why 27SA$_2$ rRNAs are involved in the formation and disappearance of ring-shaped nucleoli. We failed to observe nucleolar reshaping by

349 injecting in vitro transcribed 27SA$_2$ rRNAs into the *C. elegans* germline. It is unclear
350 whether the in vitro transcribed rRNAs could diffuse into the nucleus or require certain
351 nucleotide modifications. Previous work showed that N6-methyladenosine (m6A)
352 modification of mRNAs can also induce m6A-binding proteins to undergo LLPS (57).
353 Further investigations are required to investigate the role of 27SA2 rRNA in driving
354 nucleolar reshaping in *C. elegans*.
355
356 **Phase transition of multilayered nucleolar condensates.**
357 According to the reentrant phase transition model, condensation is driven by
358 electrostatic attraction between the negatively charged RNAs and the positively charged
359 R/G-rich IDR polypeptide (51). However, excess negatively charged RNAs lead to the
360 accumulation of a large number of counterions on the surface of the positively charged
361 polypeptide, which triggers long-range electrostatic repulsion to prevent protein
362 condensation (51, 53). An interplay between short-range cation−π attraction and long-
363 range electrostatic repulsion may tune the reentrant phase transition (52). The charge
364 balance of electrostatic interactions may be crucial for retaining transcriptional
365 condensate in vivo (58). Based on these studies, we speculated that knocking down
366 class I RPL may accumulate 27SA2 rRNAs and invert charges of nucleolar
367 ribonucleoproteins, resulting in nucleolar reshaping.
368
369 Alternatively, nucleolar subcompartments may be formed by distinct protein
370 droplets with different surface tensions (4, 8). For instance, HSP70 family proteins are
371 enriched in the center of hollow condesation and retain the morphology of TDP43
372 spherical shells (56). The nucleolar vacuole of *C. elegans* was enriched with many
373 nucleoplasmic proteins. Whether these nucleoplasmic proteins are involved in
374 nucleolar reshaping is unclear. It will be very interesting to test whether the morphology
375 of the ring-shaped nuceloli ring is maintained by certain specific proteins in the
376 nucleolar vacuole or some disordered proteins on the nucleolar ring.
377
378 Previous reports have shown that the inhibition of nucleolar function can

dramatically alter its structure (54, 59). Here, the inhibition of RNAP I by actinomycin D prohibited the formation of ring-shaped nucleoli, yet the mechanism is unclear. *C. elegans* exhibits different proportions of nucleolar ring structures in distinct tissues. Whether and how development and environmental stimuli reshape nucleolar structure require further investigation.

The function of nucleolar vacuoles

The nucleolar vacuole is an evolutionarily conserved nucleolar subcompartment, but its function remains unclear. It has been speculated that the size of the vacuole represents nucleolar activities in plants (15, 16). We found that a certain proportion of nucleoli in various tissues in wild-type *C. elegans* were ring-shaped with nucleolar vacuoles inside. In intestinal cells, approximately 90% of the nucleoli have vacuole structures from larva to gravid adult. Of note, the nucleolar vacuole in the germline nucleoli revealed dynamic changes during aging. Interestingly, during germline development, an mRNA transporter, NXF-1, was specifically enriched in the nucleolar vacuole of the germline in gravid adult worms. Furthermore, the nucleolar vacuole was enriched with many nucleoplasmic proteins. Although the nucleolar ring barriers the vacuole with the nucleoplasm, there is rapid component exchange between these two compartments. These data suggested that nucleolar vacuoles may have important roles in germline development or mRNA metabolism. Consistently, previous studies have shown that nucleolar vacuoles may be involved in the transport of nucleolar substances from the nucleolus to the nucleoplasm and temporary storage of certain materials (12, 13, 22). In tobacco BY-2 cells, time-lapse photography revealed that the nucleolar vacuole slowly disappears over time (22). We also observed a dynamic change in nucleolar vacuoles over time in the oocyte nucleoli of *C. elegans*, suggesting that the vacuole is not a simple place for material storage but rather plays important regulatory roles.

Materials and Methods

Strains.

Bristol strain N2 was used as the standard wild-type strain. All strains were grown at 20°C unless otherwise specified. The strains used in this study are listed in Supplementary Table S3.

Candidate-based RNAi screening.

RNAi experiments were performed at 20°C by placing synchronized embryos on feeding RNAi plates as previously described (60). HT115 bacteria expressing the empty vector L4440 (a gift from A. Fire) were used as controls. Bacterial clones expressing double-stranded RNAs (dsRNAs) were obtained from the Ahringer RNAi library (61) and sequenced to verify their identity. Some bacterial clones were constructed in this work, which are listed in Supplementary Table S4. All RNAi feeding experiments were performed for two generations except for larval arrest or sterile worms.

Imaging

Images were collected using a Leica DM4 microscope.

Construction of plasmids and transgenic strains.

For ectopic transgenes, the promoter and CDS region and UTR were amplified from N2 genomic DNA. The mCherry coding sequence was amplified from PFCJ90. The vector fragment was PCR amplified from plasmid pSG274. These fragments were joined together by Gibson assembly to form the repair plasmid with the ClonExpress MultiS One Step Cloning Kit (Vazyme Biotech, Nanjing, China, Cat. No. C113-01/02). The transgene was integrated into *C. elegans* chromosome II via a modified counterselection (cs)-CRISPR method. The sequences of the primers are listed in Supplementary Table S5.

For in situ knock-in transgenes, the 3xFLAG::GFP coding region was PCR

amplified from shg1248 genomic DNA. The GFP::3xFLAG coding region was PCR amplified from shg2123 genomic DNA. The mCherry coding region was PCR amplified from shg1660 genomic DNA. The tagRFP coding region was PCR amplified from YY1446 genomic DNA. Homologous left and right arms (1.5 kb) were PCR amplified from N2 genomic DNA. The backbone was PCR amplified from the plasmid pCFJ151. All these fragments were joined together by Gibson assembly to form the repair plasmid with the ClonExpress MultiS One Step Cloning Kit (Vazyme Biotech, Nanjing, China, Cat. No. C113-01/02). This plasmid was coinjected into N2 animals with three sgRNA expression vectors, 5 ng/µl pCFJ90 and the Cas9 II-expressing plasmid. The sequences of the primers are listed in Supplementary Table S6.

CRISPR/Cas9-mediated gene editing

For the *nucl-1(ust313)* in-frame mutant, a 1.5 kb homologous left arm was PCR amplified with the primers 5′-GGGTAACGCCAGCACGTGTGGCCAAAGTTTAATCACCTCGCTCGC-3’ and 5’-TCGCTAAAACCAACTCGGCTTGAGTCGAAACCCATTTTGATTGTACC-3’. A 1 kb homologous right arm was PCR amplified with the primers 5′-AGCCGAGTTGGTTTTAGCGATAAGAGAAAACAGTATGATAG-3’ and 5’-CAGCGGATAACAATTTCACATCATCTTCATCCTCATCGTC-3’. The backbone was PCR amplified from the plasmid pCFJ151 with the primers 5′-CACACGTGCTGGCGTTACCC-3′ and 5′-TGTGAAATTGTTATCCGCTGG-3′. All these fragments were joined together by Gibson assembly to form the *nucl-1* plasmid with the ClonExpress MultiS One Step Cloning Kit (Vazyme Biotech, Nanjing, China, Cat. No. C113-01/02). This plasmid was coinjected into N2 animals with three sgRNA expression vectors, *nucl-1* sgRNA#1/#2/#3, 5 ng/µl pCFJ90 and Cas9 II expressing plasmid.

The sgRNAs used in this study for transgene construction are listed in Supplementary Table S7.

Actinomycin D treatment

Actinomycin D (MedChemExpress no. HY-17559, CAS:50-76–0) was prepared at 20 mg/ml in DMSO as a stock solution. Each 3.5 µl actinomycin D stock solution was diluted with 300 µl Luria-Bertani liquid medium and layered onto NGM and RNAi plates. NGM and RNAi plates were prepared and placed at 37°C overnight before use. Synchronized L1 worms were placed onto the seeded plates and grown for 48 h before imaging and collection for cRT-PCR.

Fluorescence recovery after photobleaching (FRAP).

FRAP experiments were performed using a Zeiss LSM980 laser scanning confocal microscope at room temperature. Worms were anesthetized with 2 mM levamisole. A region of interest was bleached with 100% laser power for 3-4 seconds, and the fluorescence intensities in these regions were collected every 5 s and normalized to the initial intensity before bleaching. For analysis, image intensity was measured by Mean and further analyzed by Origin software.

DAPI staining

DNA was stained with DAPI Staining Solution (10 µg/ml) (Biosharp, BL105A) at room temperature. Worms were fixed with 1% formaldehyde before staining and soaked in DAPI solution for 3-5 minutes. After washing with phosphate-buffered saline (PBS) 2-3 times, worms were imaged under a fluorescence microscope.

RNA staining

RNA was stained with SYTO™ RNASelect™ Green Fluorescent Cell Stain (SYTO™ RNASelect™ Green Fluorescent Cell Stain-5 mM Solution in DMSO, S32703, Thermo). Worms were fixed in prechilled methanol at –20°C for 10 minutes before staining and then washed twice for 5 minutes each in PBS. The labeling solution consisted of 500 nM RNA Select Green fluorescent cell stain in phosphate-buffered

saline (PBS). Worms were soaked in the 500 nM labeling solution for 20 min at room temperature, washed twice in PBS for 5 min each, and then imaged.

cRT-PCR

Total RNA was isolated from L3 stage worms using a Dounce homogenizer (pestle B) in TRIzol solution (Invitrogen). Two micrograms of total RNA was circularized by a T4 RNA Ligase 1 Kit (M0204. NEB) and then purified by TRIzol reagent followed by isopropanol precipitation. The circularized RNA was reverse transcribed via the GoScript™ Reverse Transcription System (Promega #A5001). PCR was performed using 2 × Rapid Taq Master Mix (Vazyme, P222-01) for 25 cycles. The primer sets used in this work are listed in Supplementary Table S8.

Quantitative real-time PCR

All quantitative real-time PCR (qPCR) experiments were performed using a MyIQ2 machine (Bio-Rad). DNA or cDNA was quantified with SYBR Green Master Mix (Vazyme, Q111-02), and qPCR was performed according to the vendor's instructions. RNA was first circularized by a T4 RNA Ligase 1 Kit (M0204. NEB) and then purified by TRIzol reagent followed by isopropanol precipitation, and then reverse transcribed via GoScript™ Reverse Transcription System (Promega #A5001) with indicated primers. The primer sets used in this work are listed in Supplementary Table S8.

Statistics

Boxplots are presented with median and minimum and maximum. All of the experiments were conducted with independent *C. elegans* animals for the indicated N times. Statistical analysis was performed with the two-tailed Student's t test.

ACKNOWLEDGMENTS.

We are grateful to the members of the Guang laboratory for their comments and to

Ruining Cai from the Institute of Oceanology, Chinese Academy of Sciences, Qingdao, China. We are grateful to the International C. elegans Gene Knockout Consortium and the National Bioresource Project for providing the strains. Some strains were provided by the Caenorhabditis Genetics Center (CGC), which is funded by the NIH Office of Research Infrastructure Programs (Grant P40 OD010440). This work was supported by grants from the National Key R&D Program of China (2022YFA1302700, 2019YFA0802600), the National Natural Science Foundation of China (32230016, 91940303, 32270583, 32070619, 31870812, 31871300 and 31900434), and the Strategic Priority Research Program of the Chinese Academy of Sciences (XDB39010600). This study was supported in part by the Fundamental Research Funds for the Central Universities.

References

1. B. McStay, Nucleolar organizer regions: genomic 'dark matter' requiring illumination. *Genes Dev* **30**, 1598-1610 (2016).
2. P. J. Thul *et al.*, A subcellular map of the human proteome. *Science* **356** (2017).
3. L. Stenstrom *et al.*, Mapping the nucleolar proteome reveals a spatiotemporal organization related to intrinsic protein disorder. *Mol Syst Biol* **16**, e9469 (2020).
4. M. Feric *et al.*, Coexisting Liquid Phases Underlie Nucleolar Subcompartments. *Cell* **165**, 1686-1697 (2016).
5. C. P. Brangwynne, T. J. Mitchison, A. A. Hyman, Active liquid-like behavior of nucleoli determines their size and shape in Xenopus laevis oocytes. *Proceedings of the National Academy of Sciences of the United States of America* **108**, 4334-4339 (2011).
6. S. C. Weber, C. P. Brangwynne, Inverse Size Scaling of the Nucleolus by a Concentration-Dependent Phase Transition. *Current Biology* **25**, 641-646 (2015).
7. D. L. J. Lafontaine, J. A. Riback, R. Bascetin, C. P. Brangwynne, The nucleolus as a multiphase liquid condensate. *Nature Reviews Molecular Cell Biology* **22**, 165-182 (2021).
8. T. Kaur *et al.*, Sequence-encoded and composition-dependent protein-RNA interactions control multiphasic condensate morphologies. *Nature Communications* **12** (2021).
9. E. L. Spaulding, A. M. Feidler, L. A. Cook, D. L. Updike, RG/RGG repeats in the C. elegans

562 homologs of Nucleolin and GAR1 contribute to sub-nucleolar phase separation. *Nat*
563 *Commun* **13**, 6585 (2022).
564 10. P. J. Shaw, J. W. Brown, Plant nuclear bodies. *Curr Opin Plant Biol* **7**, 614-620 (2004).
565 11. T. H. Montgomery, *Comparative cytological studies with especial regard to the*
566 *morphology of the nucleolus*, Added t -p , Publications of the University of Pennsylvania
567 Contributions from the Zoo¨logical Laboratory for the year 1899 (Ginn & Company,
568 Boston,, 1898), pp. 2 p. l., 256 -582 p.
569 12. J. M. Johnson, L. E. Jones, Behavior of Nucleoli and Contracting Nucleolar Vacuoles in
570 Tobacco Cells Growing in Microculture. *American Journal of Botany* **54**, 189-& (1967).
571 13. R. J. Rose, G. Setterfield, L. C. Fowke, Activation of nucleoli in tuber slices and the function
572 of nucleolar vacuoles. *Exp Cell Res* **71**, 1-16 (1972).
573 14. T. Kruger, U. Scheer, p53 localizes to intranucleolar regions distinct from the ribosome
574 production compartments. *J Cell Sci* **123**, 1203-1208 (2010).
575 15. D. Stepinski, Functional ultrastructure of the plant nucleolus. *Protoplasma* **251**, 1285-1306
576 (2014).
577 16. D. Stepinski, Nucleolar vacuolation in soybean root meristematic cells during recovery
578 after chilling. *Biologia Plantarum* **52**, 507-512 (2008).
579 17. K. Hayashi, S. Matsunaga, Heat and chilling stress induce nucleolus morphological
580 changes. *Journal of Plant Research* **132**, 395-403 (2019).
581 18. J. M. Johnson, A Study of Nucleolar Vacuoles in Cultured Tobacco Cells Using
582 Radioautography, Actinomycin D, and Electron Microscopy. *Journal of Cell Biology* **43**,
583 197-& (1969).
584 19. T. Debarsy, R. Deltour, R. Bronchart, Study of Nucleolar Vacuolation and Rna-Synthesis in
585 Embryonic Root Cells of Zea-Mays. *Journal of Cell Science* **16**, 95-112 (1974).
586 20. A. F. Beven, G. G. Simpson, J. W. Brown, P. J. Shaw, The organization of spliceosomal
587 components in the nuclei of higher plants. *J Cell Sci* **108 (Pt 2)**, 509-518 (1995).
588 21. A. F. Beven *et al.*, The organization of ribosomal RNA processing correlates with the
589 distribution of nucleolar snRNAs. *Journal of Cell Science* **109**, 1241-1251 (1996).
590 22. S. L. Reichow, T. Hamma, A. R. Ferre-D'Amare, G. Varani, The structure and function of
591 small nucleolar ribonucleoproteins. *Nucleic Acids Research* **35**, 1452-1464 (2007).
592 23. C. Zhu *et al.*, Erroneous ribosomal RNAs promote the generation of antisense ribosomal
593 siRNA. *Proc Natl Acad Sci U S A* **115**, 10082-10087 (2018).
594 24. K. M. Ruff, S. Roberts, A. Chilkoti, R. V. Pappu, Advances in Understanding Stimulus
595 Responsive Phase Behavior of Intrinsically Disordered Protein Polymers. *Journal of*
596 *Molecular Biology* **430**, 4619-4635 (2018).
597 25. A. Bremer *et al.*, Deciphering how naturally occurring sequence features impact the phase
598 behaviours of disordered prion-like domains. *Nature Chemistry* **14**, 196-+ (2022).
599 26. E. W. Martin *et al.*, Valence and patterning of aromatic residues determine the phase
600 behavior of prion-like domains. *Science* **367**, 694-+ (2020).
601 27. P. Pullara, I. Alshareedah, P. R. Banerjee, Temperature-dependent reentrant phase
602 transition of RNA-polycation mixtures. *Soft Matter* **18**, 1342-1349 (2022).
603 28. S. Liao *et al.*, Antisense ribosomal siRNAs inhibit RNA polymerase I-directed transcription
604 in C. elegans. *Nucleic Acids Res* **49**, 9194-9210 (2021).
605 29. X. Zhou *et al.*, RdRP-synthesized antisense ribosomal siRNAs silence pre-rRNA via the

nuclear RNAi pathway. *Nat Struct Mol Biol* **24**, 258-269 (2017).

30. W. Yokoyama *et al.*, rRNA adenine methylation requires T07A9.8 gene as rram-1 in Caenorhabditis elegans. *Journal of Biochemistry* **163**, 465-474 (2018).
31. D. Korcekova, A. Gombitova, I. Raska, D. Cmarko, C. Lanctot, Nucleologenesis in the Caenorhabditis elegans embryo. *PLoS One* **7**, e40290 (2012).
32. O. Zatsepina, C. Baly, M. Chebrout, P. Debey, The step-wise assembly of a functional nucleolus in preimplantation mouse embryos involves the Cajal (coiled) body. *Developmental Biology* **253**, 66-83 (2003).
33. E. Saijou, T. Fujiwara, T. Suzaki, K. Inoue, H. Sakamoto, RBD-1, a nucleolar RNA-binding protein, is essential for Caenorhabditis elegans early development through 18S ribosomal RNA processing. *Nucleic Acids Research* **32**, 1028-1036 (2004).
34. G. Wan, J. Yan, Y. H. Fei, D. J. Pagano, S. Kennedy, A Conserved NRDE-2/MTR-4 Complex Mediates Nuclear RNAi in Caenorhabditis elegans. *Genetics* **216**, 1071-1085 (2020).
35. A. Akay *et al.*, The Helicase Aquarius/EMB-4 Is Required to Overcome Intronic Barriers to Allow Nuclear RNAi Pathways to Heritably Silence Transcription. *Developmental Cell* **42**, 241-+ (2017).
36. S. Guang *et al.*, An Argonaute transports siRNAs from the cytoplasm to the nucleus. *Science* **321**, 537-541 (2008).
37. S. H. Guang *et al.*, Small regulatory RNAs inhibit RNA polymerase II during the elongation phase of transcription. *Nature* **465**, 1097-U1165 (2010).
38. U. Sheth, J. Pitt, S. Dennis, J. R. Priess, Perinuclear P granules are the principal sites of mRNA export in adult C. elegans germ cells. *Development* **137**, 1305-1314 (2010).
39. A. F. Pendle *et al.*, Proteomic analysis of the Arabidopsis nucleolus suggests novel nucleolar functions. *Molecular Biology of the Cell* **16**, 260-269 (2005).
40. M. Gamalinda *et al.*, A hierarchical model for assembly of eukaryotic 60S ribosomal subunit domains. *Genes & Development* **28**, 198-210 (2014).
41. R. L. Hang *et al.*, Ribosomal RNA Biogenesis and Its Response to Chilling Stress in Oryza sativa. *Plant Physiology* **177**, 381-397 (2018).
42. M. Zakrzewska-Placzek, F. F. Souret, G. J. Sobczyk, P. J. Green, J. Kufel, Arabidopsis thaliana XRN2 is required for primary cleavage in the pre-ribosomal RNA. *Nucleic Acids Research* **38**, 4487-4502 (2010).
43. H. W. Gabel, G. Ruvkun, The exonuclease ERI-1 has a conserved dual role in 5.8S rRNA processing and RNAi. *Nat Struct Mol Biol* **15**, 531-533 (2008).
44. N. Hiraishi, Y. Ishida, H. Sudo, M. Nagahama, WDR74 participates in an early cleavage of the pre-rRNA processing pathway in cooperation with the nucleolar AAA-ATPase NVL2. *Biochemical and Biophysical Research Communications* **495**, 116-123 (2018).
45. E. W. Horsey, E. Jakovljevic, T. D. Miles, P. Harnpicharnchai, J. L. Woolford, Role of yeast Rrp1 protein in the dynamics of pre-ribosome maturation. *Rna* **10**, 813-827 (2004).
46. P. G. Yang *et al.*, G3BP1 Is a Tunable Switch that Triggers Phase Separation to Assemble Stress Granules. *Cell* **181**, 325-+ (2020).
47. S. Elbaum-Garfinkle *et al.*, The disordered P granule protein LAF-1 drives phase separation into droplets with tunable viscosity and dynamics. *Proceedings of the National Academy of Sciences of the United States of America* **112**, 7189-7194 (2015).
48. P. A. Chong, R. M. Vernon, J. D. Forman-Kay, RGG/RG Motif Regions in RNA Binding and

Phase Separation. *J Mol Biol* **430**, 4650-4665 (2018).

49. H. Ginisty, H. Sicard, B. Roger, P. Bouvet, Structure and functions of nucleolin. *J Cell Sci* **112 (Pt 6)**, 761-772 (1999).

50. F. Frottin *et al.*, The nucleolus functions as a phase-separated protein quality control compartment. *Science* **365**, 342-347 (2019).

51. P. R. Banerjee, A. N. Milin, M. M. Moosa, P. L. Onuchic, A. A. Deniz, Reentrant Phase Transition Drives Dynamic Substructure Formation in Ribonucleoprotein Droplets. *Angewandte Chemie-International Edition* **56**, 11354-11359 (2017).

52. I. Alshareedah *et al.*, Interplay between Short-Range Attraction and Long-Range Repulsion Controls Reentrant Liquid Condensation of Ribonucleoprotein-RNA Complexes. *Journal of the American Chemical Society* **141**, 14593-14602 (2019).

53. I. Alshareedah, M. M. Moosa, M. Raju, D. A. Potoyan, P. R. Banerjee, Phase transition of RNA-protein complexes into ordered hollow condensates. *Proceedings of the National Academy of Sciences of the United States of America* **117**, 15650-15658 (2020).

54. Y. Shav-Tal *et al.*, Dynamic sorting of nuclear components into distinct nucleolar caps during transcriptional inhibition. *Molecular Biology of the Cell* **16**, 2395-2413 (2005).

55. Y. D. Yin *et al.*, Non-equilibrium behaviour in coacervate-based protocells under electric-field-induced excitation. *Nature Communications* **7** (2016).

56. H. Y. Yu *et al.*, HSP70 chaperones RNA-free TDP-43 into anisotropic intranuclear liquid spherical shells. *Science* **371**, 585-+ (2021).

57. R. J. Ries *et al.*, m(6)A enhances the phase separation potential of mRNA. *Nature* **571**, 424-+ (2019).

58. J. E. Henninger *et al.*, RNA-Mediated Feedback Control of Transcriptional Condensates. *Cell* **184**, 207-+ (2021).

59. S. Boulon, B. J. Westman, S. Hutten, F. M. Boisvert, A. I. Lamond, The nucleolus under stress. *Mol Cell* **40**, 216-227 (2010).

60. L. Timmons, D. L. Court, A. Fire, Ingestion of bacterially expressed dsRNAs can produce specific and potent genetic interference in Caenorhabditis elegans. *Gene* **263**, 103-112 (2001).

61. R. S. Kamath *et al.*, Systematic functional analysis of the Caenorhabditis elegans genome using RNAi. *Nature* **421**, 231-237 (2003).

683 **Figure legends**

684 **Figure 1. Identification of two-shaped nucleoli in *C. elegans*.** (A) Schematic
685 diagram of nucleolar structure in mammals, plants and *C. elegans*. (B) Differential
686 interference contrast (DIC) and fluorescence microscopy images of *C. elegans* nucleoli
687 in the indicated tissues. (C) Quantification of ring-shaped nucleoli at the indicated
688 developmental stages. n>20 animals. (D) DIC and fluorescence microscopy images
689 of pachytene cells. (E) Quantification of ring-shaped nucleoli in the germline
690 pachytene stage. n>20 animals.

691

692 **Figure 2. Class I RPLs are required for the maintenance of nucleolar structural**
693 **integrity.** (A) Schematic diagram of the candidate RNAi-based genetic screening
694 for the formation of ring-shaped nucleoli in the *C. elegans* epidermis. (B-C) Images
695 of *C. elegans* nucleoli after knockdown of the indicated genes by RNAi in distinct
696 tissues. (D) Quantification of the ring-shaped nucleoli after RNAi knockdown of the
697 indicated genes. n>11 animals. (E) Summary of the formation of ring-shaped
698 nucleoli after knocking down Class I and II *rpl* genes. (F-K) The size of the
699 nucleolar vacuole (F-H) and nucleolar ring (I-K) after RNAi knockdown of the
700 indicated genes. n>60 nucleoli from 10 animals.

701

702 **Figure 3. rRNA transcription and processing factors accumulate at the**
703 **nucleolar ring**. (A-D) DIC and fluorescence microscopy images of the indicated
704 transgenes after knocking down *rpl-14*. (E) Summary of the localization of the
705 indicated proteins after *rpl-14* RNAi. (F) DAPI staining of epidermal cells after *rpl-*
706 *14* RNAi. (G) Fluorescent density scan of GFP:: RRP-8 and DAPI staining by
707 ImageJ. (H-J) (top) FRAP assay of transgenes in the indicated regions before and after
708 *rpl-14* RNAi. (bottom) Quantification of FRAP data. mean ± SD, n = 3.

709

710 **Figure 4. The nucleolar vacuole contains nucleoplasmic proteins.** (A-C) DIC and
711 fluorescence microscopy images of the indicated transgenes after knocking down
712 *rpl-14*. (D) Summary of the localization of the indicated proteins after *rpl-14* RNAi.
713 (E, F) (top) FRAP assay of GFP::NRDE-2 and GFP::MTR-4 in the indicated regions.
714 (bottom) Quantification of FRAP data. mean ± SD, n = 3.

715

716 **Figure 5. Class I *rpl* genes are required for $27SA_2$ rRNA processing.** (A)

Schematic diagram of circularized reverse-transcription PCR (cRT-PCR) method. (B) cRT-PCR assay of 26S pre-rRNA intermediates. (C) Sanger sequencing of the ends of $27SA_2$ and 27SB rRNAs. N represents the number of clones sequenced. (D-E) cRT-PCR assay (D) and quantification (E) of $27SA_2$ and 27SB pre-rRNA intermediates after knocking down the indicated *rpl* genes by RNAi.

Figure 6. FIB-1 and NUCL-1 are required for the formation of ring-shaped nucleoli. (A) Schematic diagram of the domain structure and predicted intrinsically disordered regions of NUCL-1 and FIB-1. (B) DIC and fluorescence microscopy images of the indicated epidermal cells upon RNAi targeting of the indicated genes. (C) Quantification of ring-shaped nucleoli in epidermal cells. n=20 animals. (D) FRAP assay of GFP::RRP-8 in *nucl-1* mutants. mean ± SD, n = 3. (E) cRT-PCR assay of $27SA_2$ and 27SB pre-rRNA intermediates after knocking down the indicated genes by RNAi. (F) cRT-PCR assay of $27SA_2$ and 27SB pre-rRNA intermediates of the nucl-1 mutant after knocking down rpl-14 by RNAi. (G) DIC and fluorescence microscopy images of the indicated epidermal cells upon *rpl-14* RNAi over time. (H) Quantification of ring-shaped nucleoli in epidermal cells. n=20 animals. (I) Expression levels of $27SA_2$ pre-rRNAs quantified by real-time PCR.

Figure 7. rRNA transcription and maturation are required for nucleolar reshaping. (A, B) DIC and fluorescence microscopy images of the indicated epidermal cells after actinomycin D (Act. D) treatment, without (A) or with (B) *rpl-14* RNAi. (C) Quantification of ring-shaped nucleoli after actinomycin D treatment in the presence of *rpl-14* RNAi. n = 20. (D) (top) cRT-PCR assay and (bottom) quantification of $27SA_2$ pre-rRNA intermediates after actinomycin D treatment in the presence of *rpl-14* RNAi. (J) A working model of rRNA intermediate-directed nucleolar reshaping.

Supplemental figure legends

Figure S1. RNAi screening identified class I RPLs inhibiting the formation of ring-shaped nucleoli. (A) Differential interference contrast (DIC) of *C. elegans* nucleoli in the indicated cells. (B-D) DIC images of *C. elegans* nucleoli after knockdown of the indicated genes by RNAi. (E) Differential interference contrast (DIC) and fluorescence microscopy images of *C. elegans* nucleoli after knockdown of the

indicated genes by RNAi in oocytes. (F) The size of nucleoli after RNAi knockdown of the indicated genes. n>60 nucleoli from 10 animals.

Figure S2. Cold stress inhibited the formation of ring-shaped nucleoli. (A-B) DIC and fluorescence microscopy images (A) and quantification (B) of ring-shaped nucleoli in intestine cells after 4°C cold stress for 12 h and recovery at 20°C for 24 h in wild-type worms. n = 20 animals. (C) DIC and fluorescence microscopy images of epidermal cells after 4°C cold stress for 12 h and recovery at 20°C for 24 h with and without *rpl-14* RNAi. (D) Quantification of ring-shaped nucleoli in epidermal cells after 4°C cold stress for 12 h and recovery at 20°C for 24 h. n = 20 animals.

Figure S3. rRNA transcription and processing factors accumulate at the nucleolar ring. (A-F) DIC and fluorescence microscopy images of the indicated transgenes after knocking down *rpl-14*. (G) SYTO RNA select staining of epidermal cells after *rpl-14* RNAi. (H) Fluorescent density scan of GFP::RRP-8 and SYTO RNA select staining by ImageJ.

Figure S4. Nucleolar vacuoles contained nucleoplasmic proteins. (A-D) DIC and fluorescence microscopy images of the indicated transgenes at the ring-shaped nucleoli in wild-type animals. (E-I) DIC and fluorescence microscopy images of the indicated transgenes after knocking down *rpl-14*. (J) (left) FRAP assay of GFP::NRDE-2. (right) Quantification of FRAP data. mean ± SD, n = 3.

Figure S5. The mRNA export factor NXF-1 is enriched in the nucleolar vacuole. (A) DIC and fluorescence microscopy images of NXF-1 in ring-shaped nucleoli in wild-type animals. (B) DIC and fluorescence microscopy images of the indicated transgenes after knocking down *rpl-14*. (C) Fluorescent density scan of RRP-8::GFP and NXF-1::mCherry by ImageJ. (D) DIC and fluorescence microscopy images of the pachytene cell nucleoli in the germline. (E) (top) Relative intensity of NXF-1::mCherry in the nucleolar vacuole vs at the nucleolar ring. mean ± SD, n = 3. (bottom) Percentage of ring-shaped nucleoli at the pachytene stage. n>20 animals.

Figure S6. cRT-PCR assay of rRNAs. (A-C) cRT-PCR assay of mature rRNAs. Ends of the mature 18S (A), 26S (B) and 5.8S (C) rRNA were PCR amplified,

785 followed by Sanger sequencing. Ends of mature 18S, 26S and 5.8S rRNA annotated
786 by Wormbase are shown. N represents the number of clones sequenced.
787
788 **Figure S7. Identification of 18S rRNA intermediates by cRT-PCR.** (A-B) cRT-
789 PCR assay of 18S rRNA rRNA intermediates upon knocking down *rps-1* and *rps-5*
790 by RNAi. (C-D) The relative positions of 18S rRNA intermediates are shown. (E-J)
791 Sanger sequencing of the ends of six 18S rRNA intermediates. The number of clones
792 sequenced is shown at the left of each panel.
793
794 **Figure S8. The accumulation of $27SA_2$ rRNA may disrupt nucleolar integrity.**
795 (A) Schematic diagram of rRNA processing in *C. elegans*. (B) Images of *C. elegans*
796 nucleoli after knockdown of the indicated genes by RNAi in the epidermis. (C)
797 Summary of the functions of the indicated genes in pre-rRNA processing. (D-E)
798 cRT-PCR assay of 26S rRNA intermediates.
799
800 **Figure S9. *nucl-1* and *fib-1* are required for the formation of ring-shaped nucleoli.**
801 (A) Predicated nucleolar proteins containing IDR and RNA binding motifs. (B)
802 Schematic diagram of NUCL-1. The deletion alleles *ust313* and *ust323* were
803 constructed by CRISPR/Cas9 technology. *ust313* was an in-frame deletion. *ust323*
804 was likely a null allele. (C) Images of *C. elegans* nucleoli after knockdown of the
805 indicated genes by RNAi in *nucl-1* mutants. (D) Quantification of the ring-shaped
806 nucleoli after RNAi knockdown of the indicated genes. n>20 animals. (E) (top) cRT-
807 PCR assay of $27SA_2$ rRNA intermediates upon knockdown of the indicated genes
808 by RNAi. (bottom) Levels of $27SA_2$ pre-rRNAs quantified by real-time PCR. mean ±
809 SD, n = 3. (F) (top) cRT-PCR assay of $27SA_2$ rRNA intermediates of the nucl-1
810 mutant upon knockdown of the indicated genes by RNAi. (bottom) Levels of $27SA_2$
811 pre-rRNAs quantified by real-time PCR. (G) cRT-PCR assay of $27SA_2$ rRNA
812 intermediates by knocking down *rpl-14*.
813
814 **Table S1. List of genes used in the candidate-based RNAi screening.**
815
816 **Table S2. List of genes involved in 26S rRNA processing.**
817
818 **Table S3: List of strains used in this study.**

819

820 **Table S4. Sequences of double-stranded RNA for RNAi screening**

821

822 **Table S5. Sequence of repair plasmid primers used in ectopic transgenic strain**
823 **construction**

824

825 **Table S6. Sequence of repair plasmid primers used in in situ transgenic strain**
826 **construction**

827

828 **Table S7. Sequences of sgRNAs for CRISPR/Cas9-mediated gene editing.**

829

830 **Table S8. Sequence of cRT-PCR and qPCR primers**

831
832

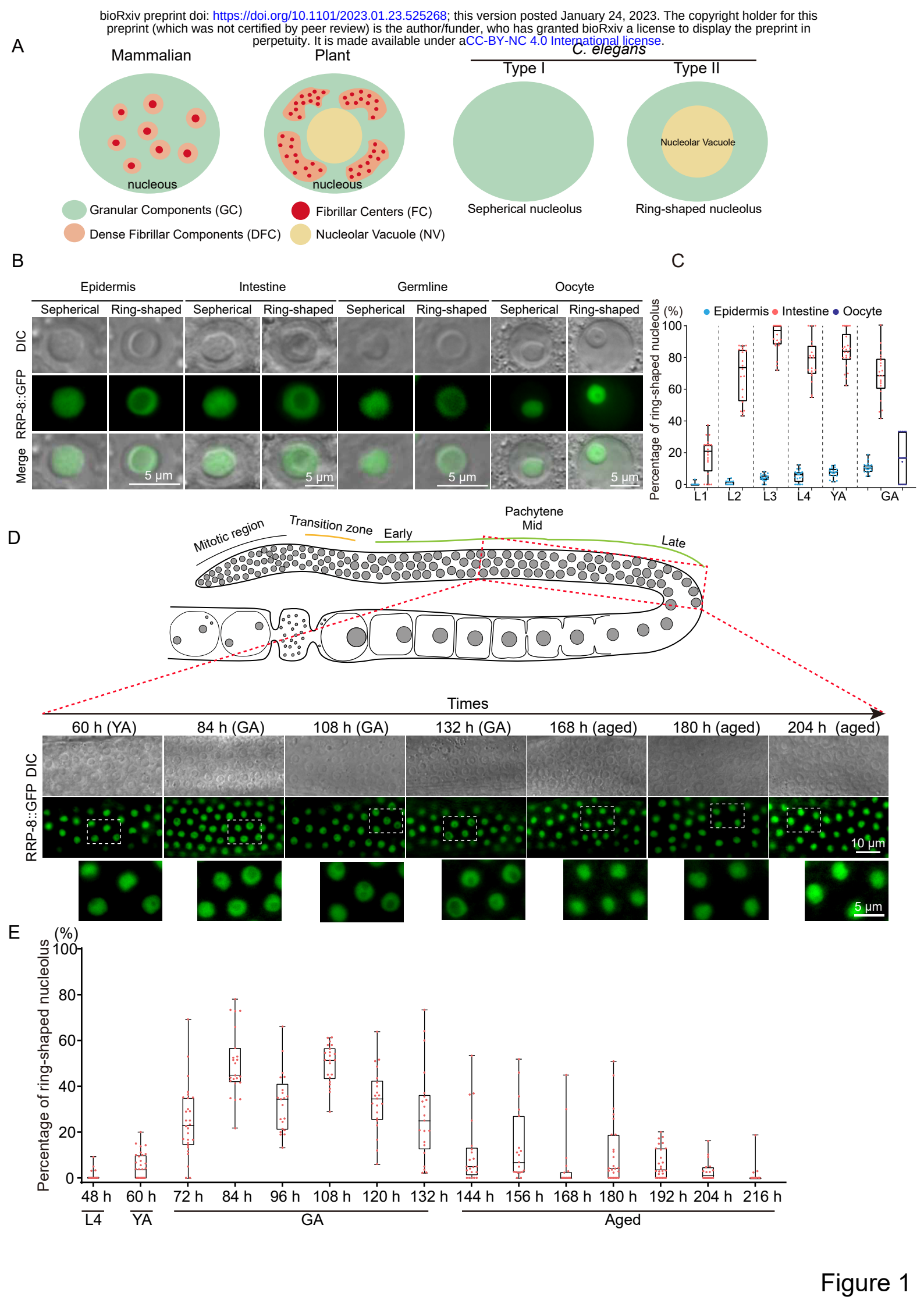

Figure 1

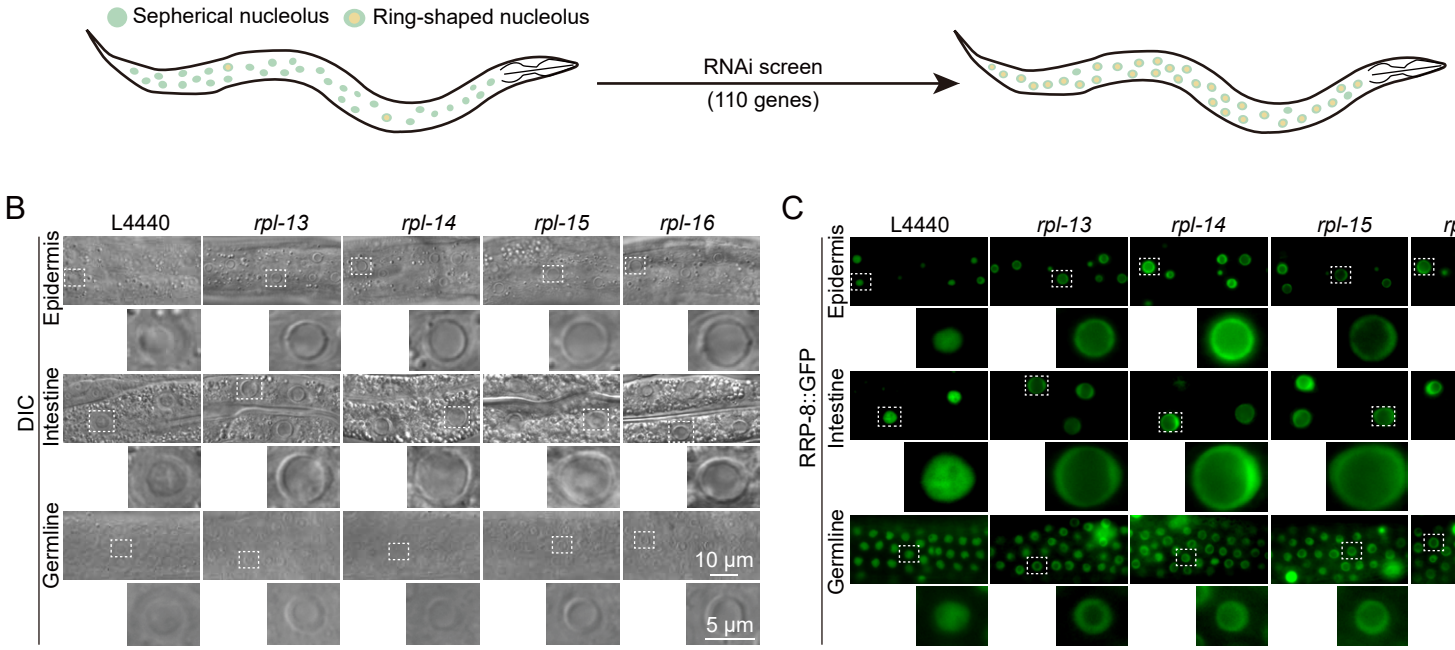

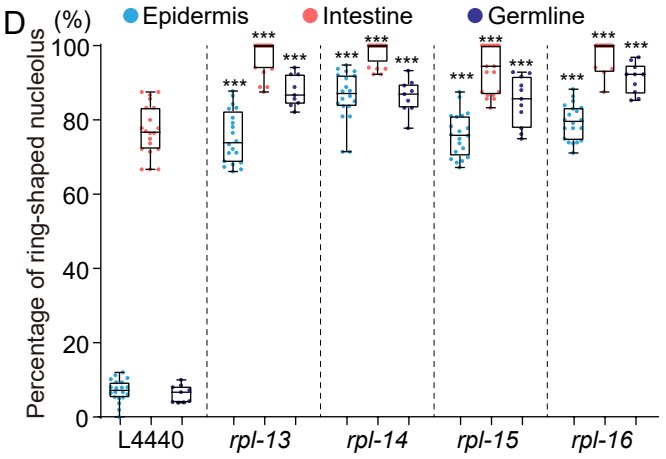

E

Type	Genes	Nucleolar Morphology
Class I	*rpl-3, rpl-4, rpl-6, rpl-7, rpl-7A, rpl-13, rpl-14, rpl-15, rpl-16, rpl-17, rpl-18, rpl-20, rpl-23, rpl-24.2, rpl-26, rpl-32, rpl-33, rpl-35, rpl-36*	ring-shaped nucleous
Class II	*rpl-1, rpl-2, rpl-5, rpl-9, rpl-10, rpl-11.1, rpl-11.2, rpl-12, rpl-19, rpl-21, rpl-22, rpl-24.1, rpl-25.1, rpl-25.2, rpl-27, rpl-28, rpl-29, rpl-30, rpl-31, rpl-34, rpl-36.A, rpl-37, rpl-38, rpl-39, rpl-40, rpl-41.1, rpl-41.2, rpl-42, rpl-43*	sepherical nucleous

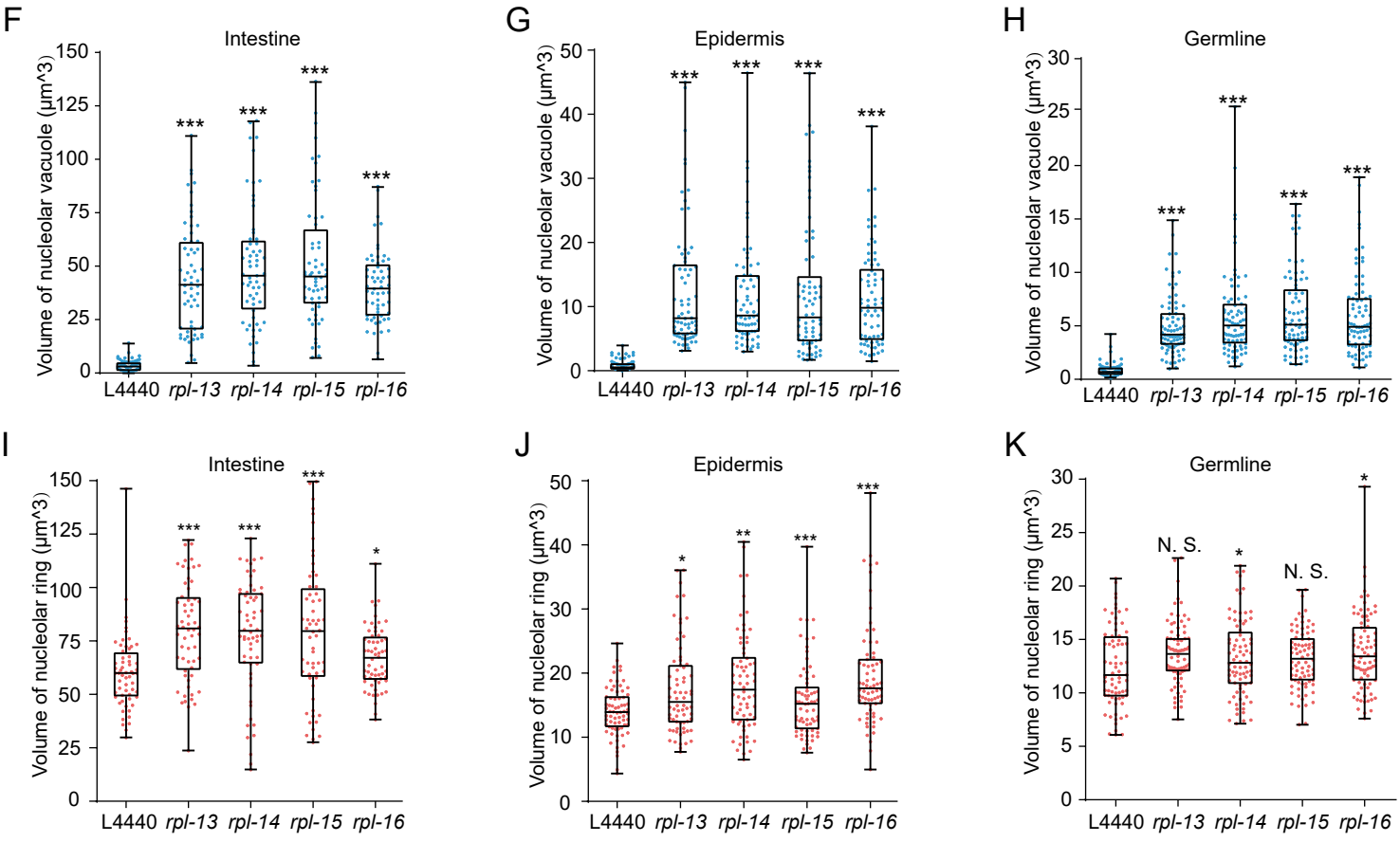

Figure 2

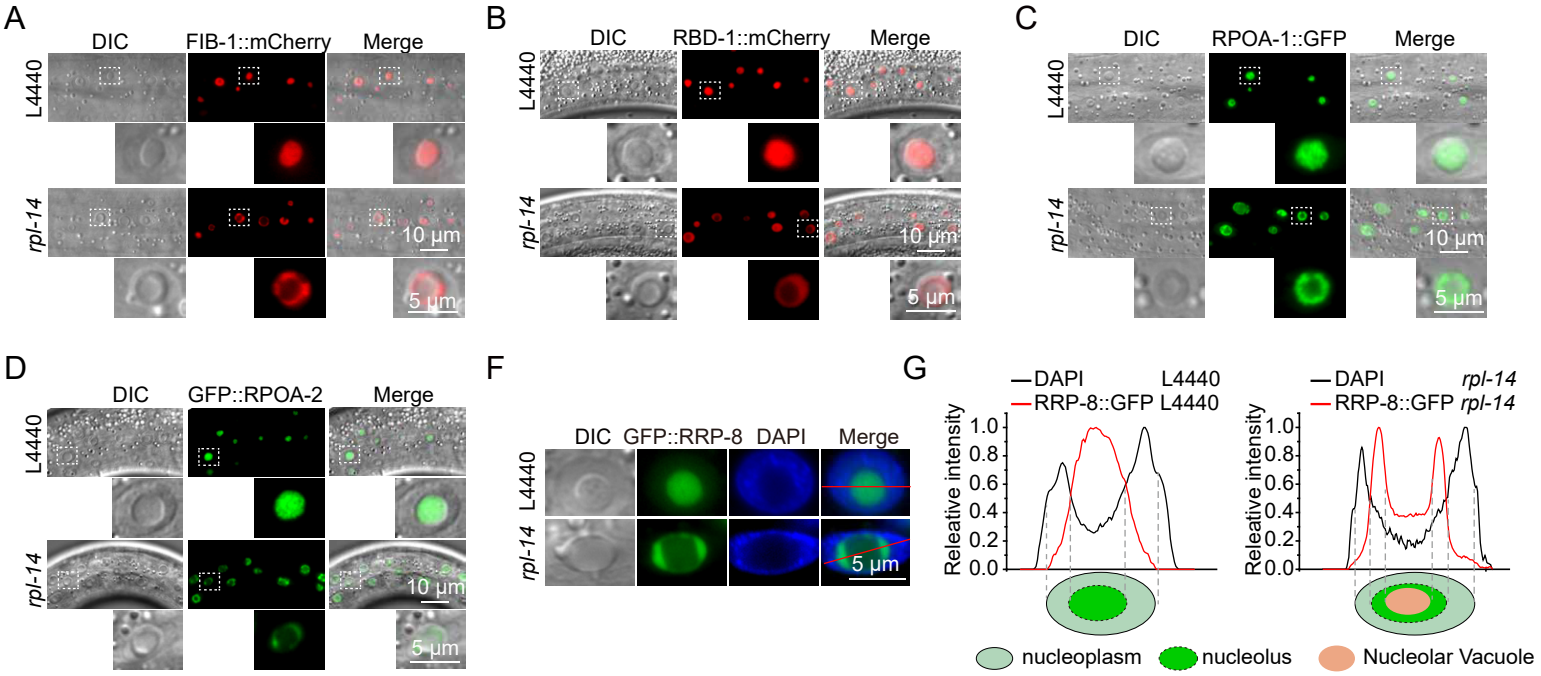

E

Proteins	Function	Localization	
		sepherical nucleolus	ring-shaped nucleolus
RRP-8	N1-methyladenosine modification of rRNA		
FIB-1	methyltransferase for pre-rRNA processing and modification		
RPOA-1	subunit of RNA polymerase I complex		
RPOA-2	subunit of RNA polymerase I complex		
RPAC-19	subunit of RNA polymerase I and III complex		
DAO-5	bind to rDNA, involved in rRNA transcription		
RPL-7	ribosomal protein, large subunit		
RBD-1	involved in 18S ribosomal RNA processing		
T06E6.1	involved in ribosomal large subunit biogenesis		

The area enclosed by the solid line is the nucleus and the area enclosed by the dotted line is the nucleolus. nucleus nucleolus

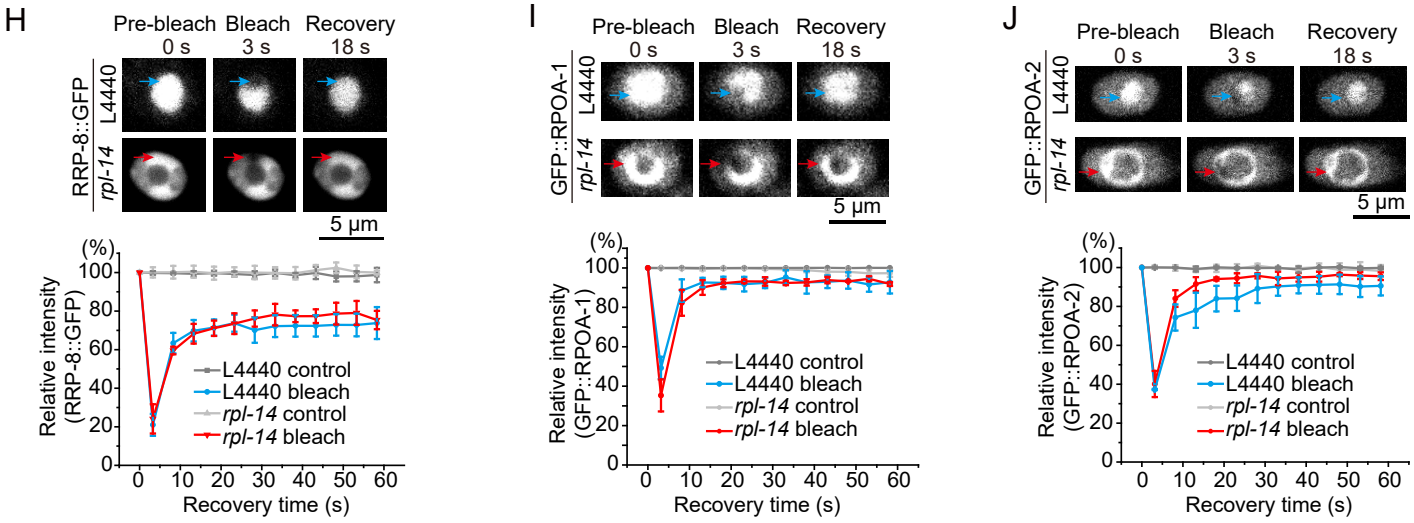

Figure 3

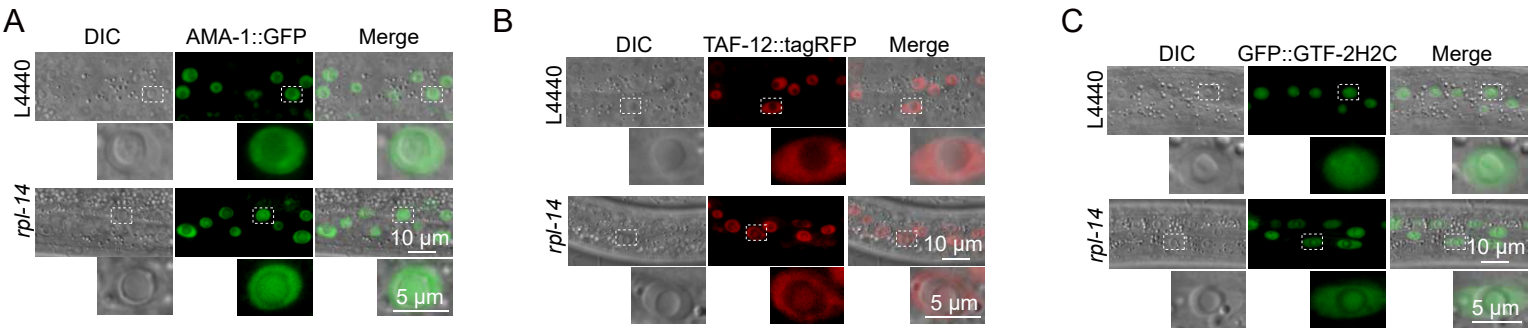

D

Proteins	Function	Location	
		sepherical nucleolus	ring-shaped nucleolus
NRDE-2	Involved in RNA interference and heterochromatin assembly		
NRDE-3	siRNA binding activity. Involved in RNA import into nucleus		
MTR-4	Involved in RNA catabolic process and maturation of 5.8S rRNA		
EMB-4	involved in pre-mRNA processing		
AMA-1	Involved in mRNA transcription by RNA polymerase II		
TAF-12	Subunit of transcription factor TFIID complex		
GTF-2H2C	Subunit of transcription factor TFIIH holo complex		
HIS-71	Ortholog of human H3-3B		
NXF-1	Involved in mRNA export from nucleus		
EXOS-2	Subunit of RNA exosome		

The area enclosed by the solid line is the nucleus and the area enclosed by the dotted line is the nucleolus nucleus nucleolus

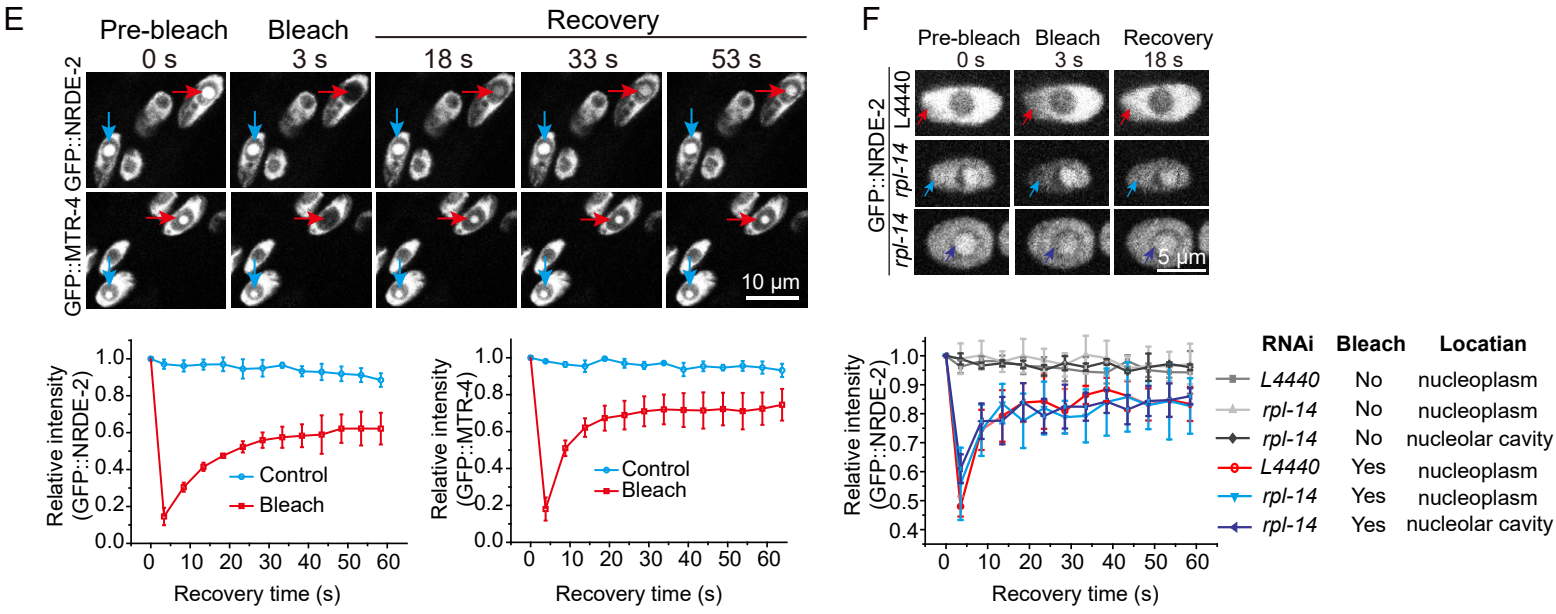

Figure 4

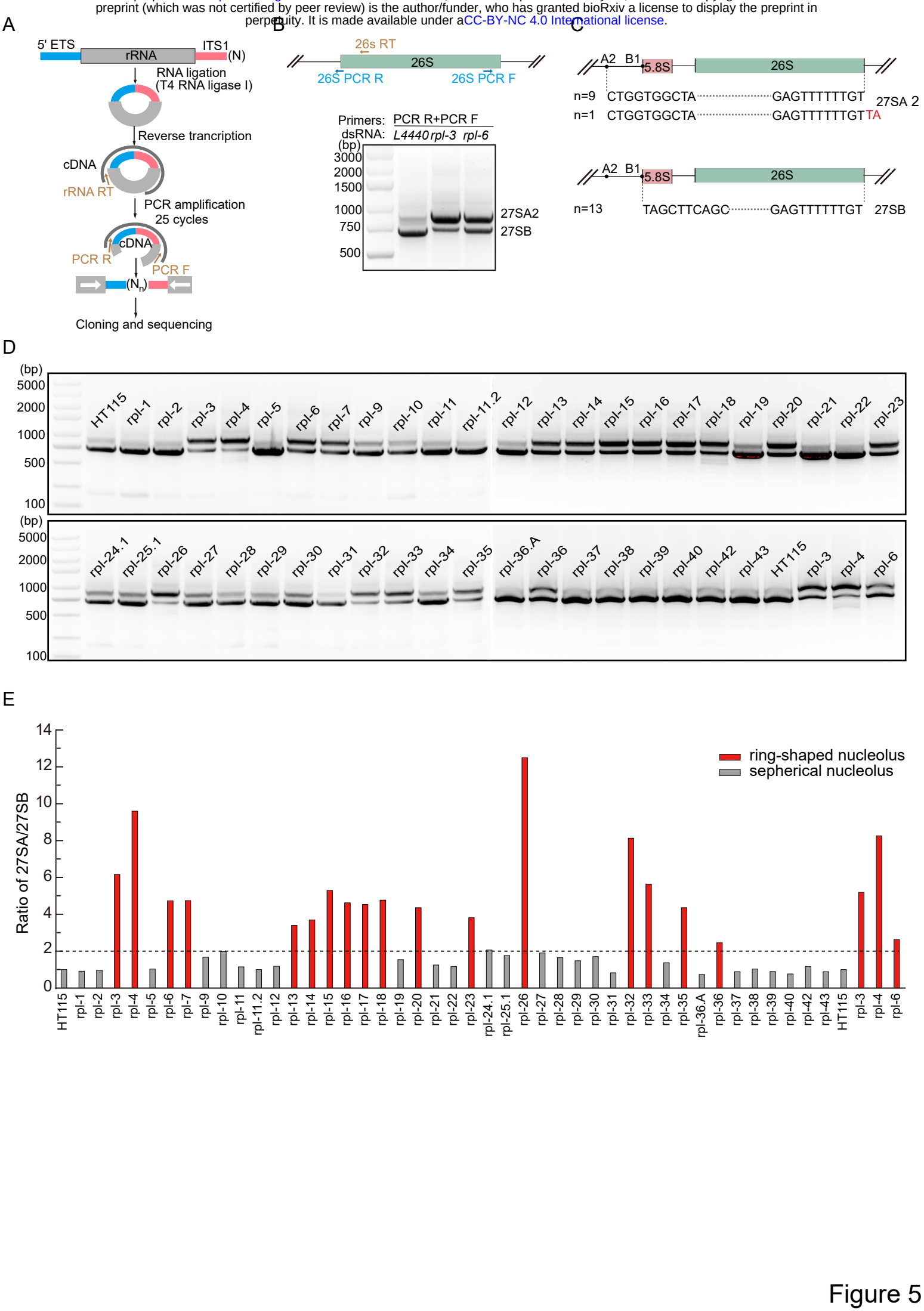

Figure 5

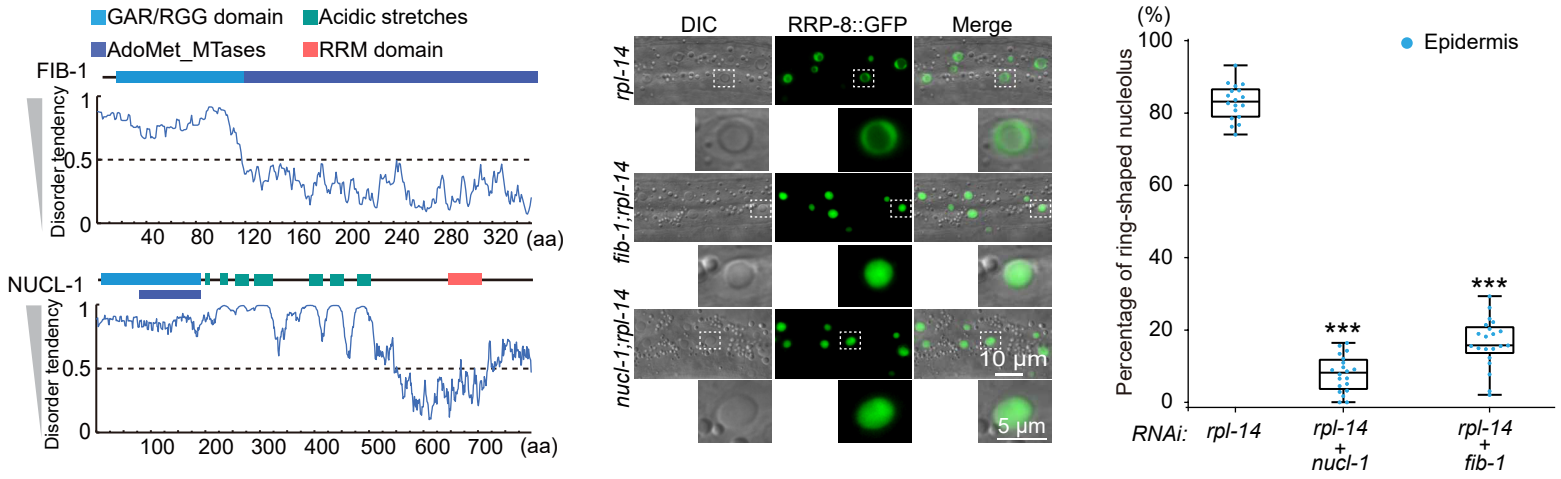

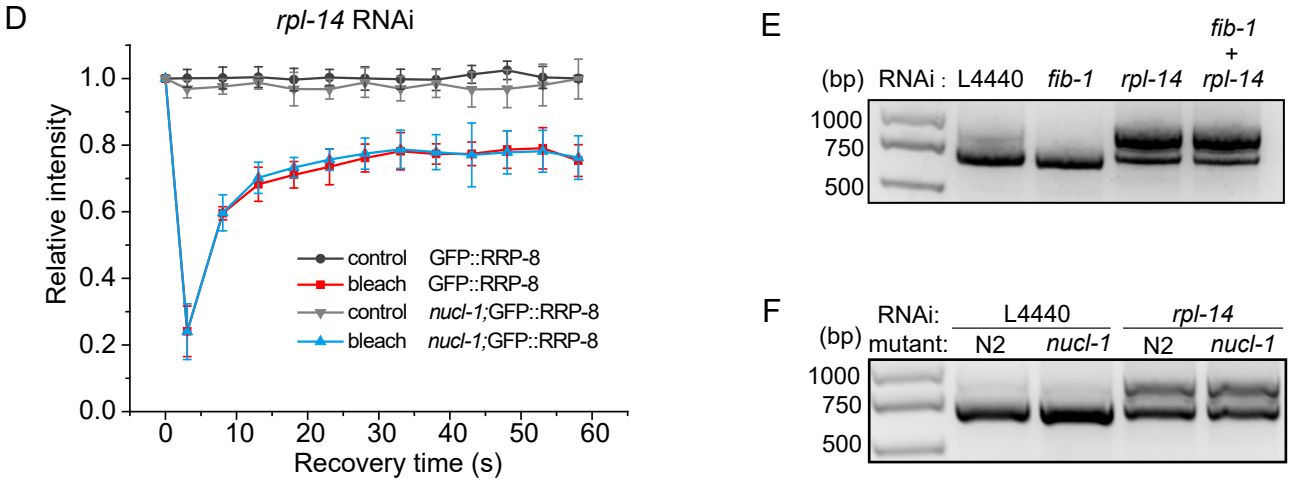

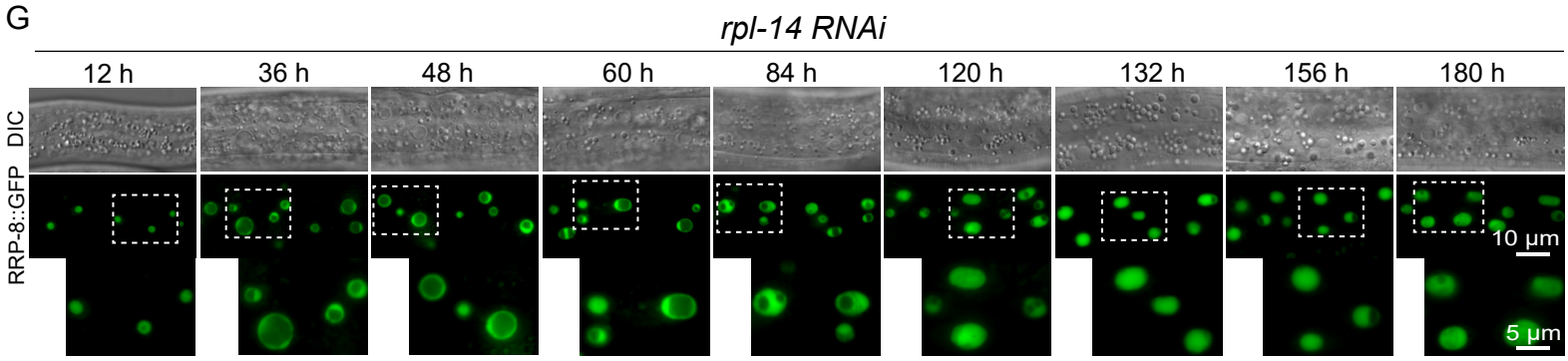

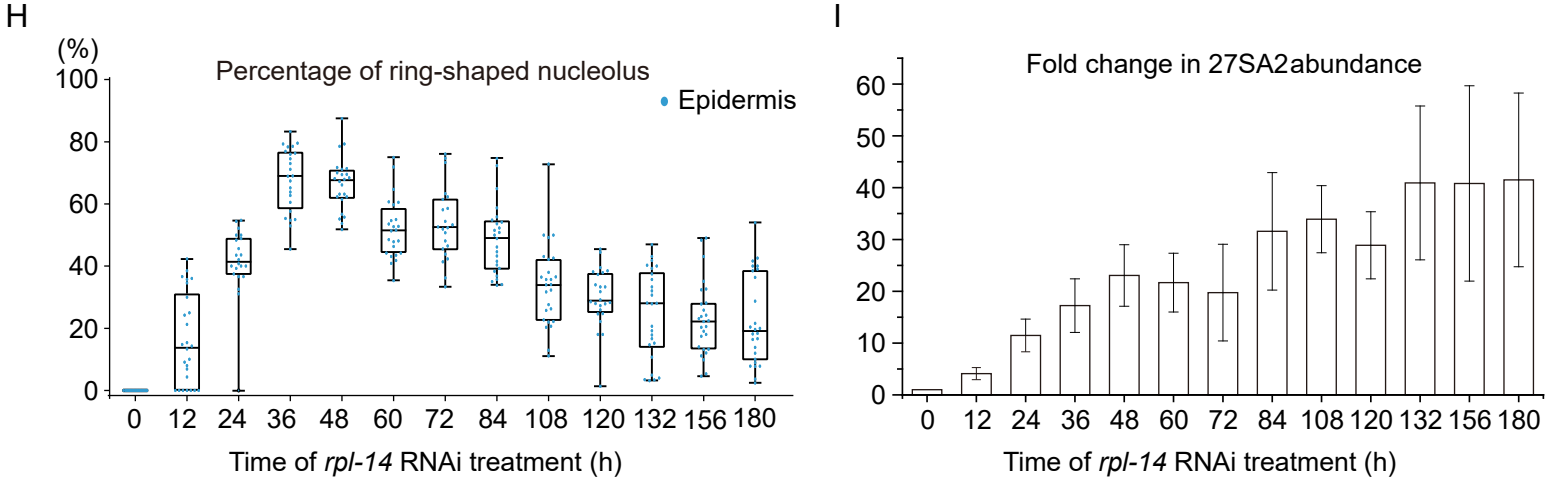

Figure 6

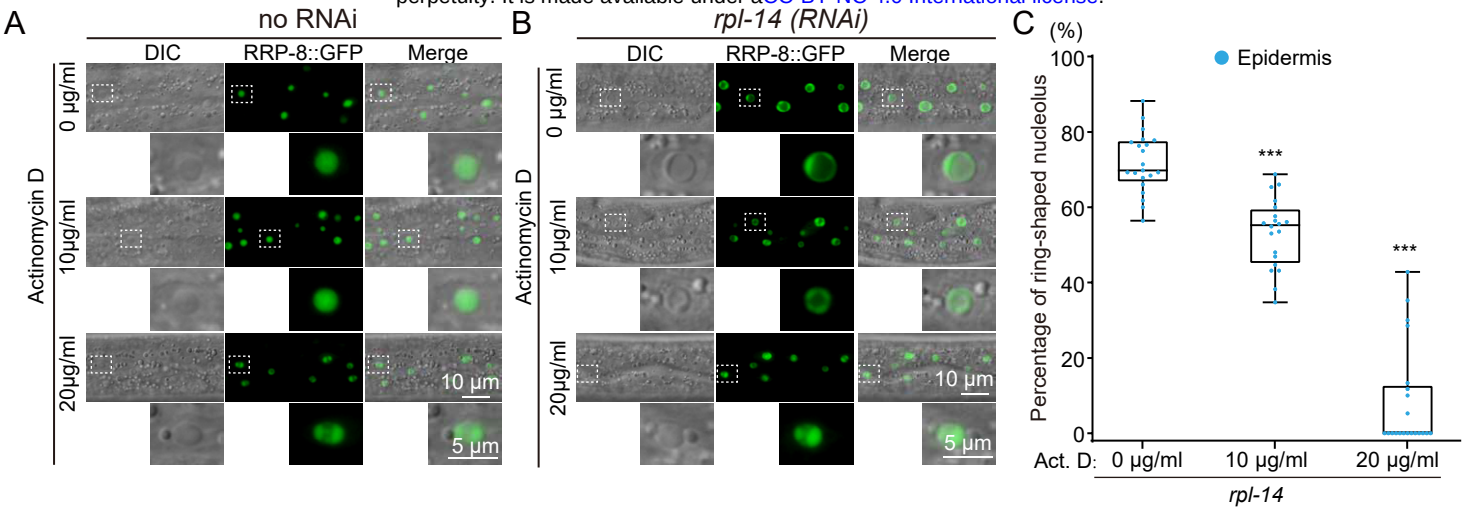

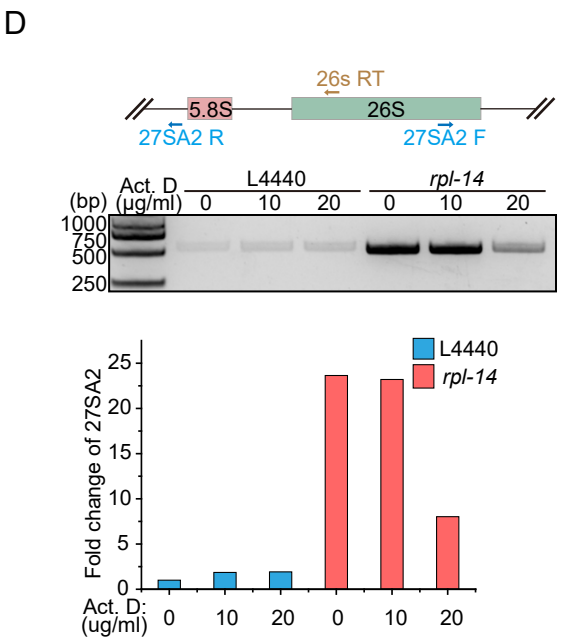

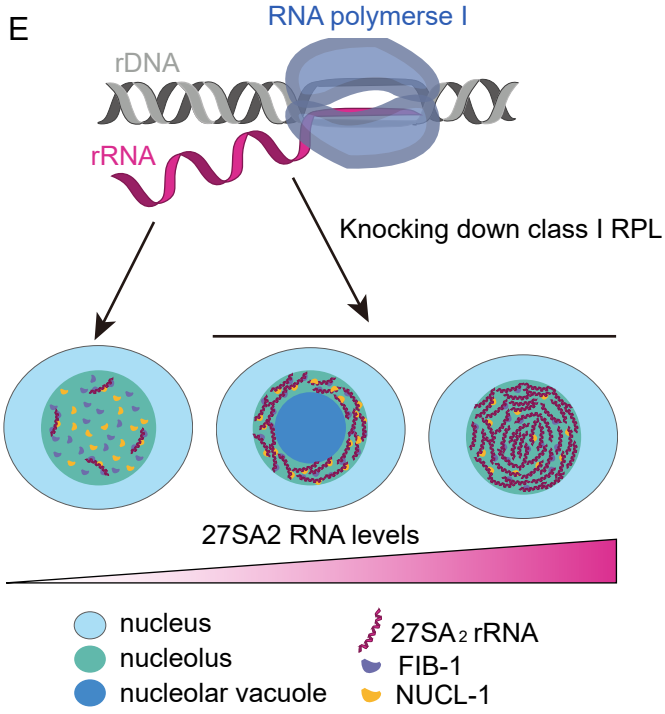

Figure 7

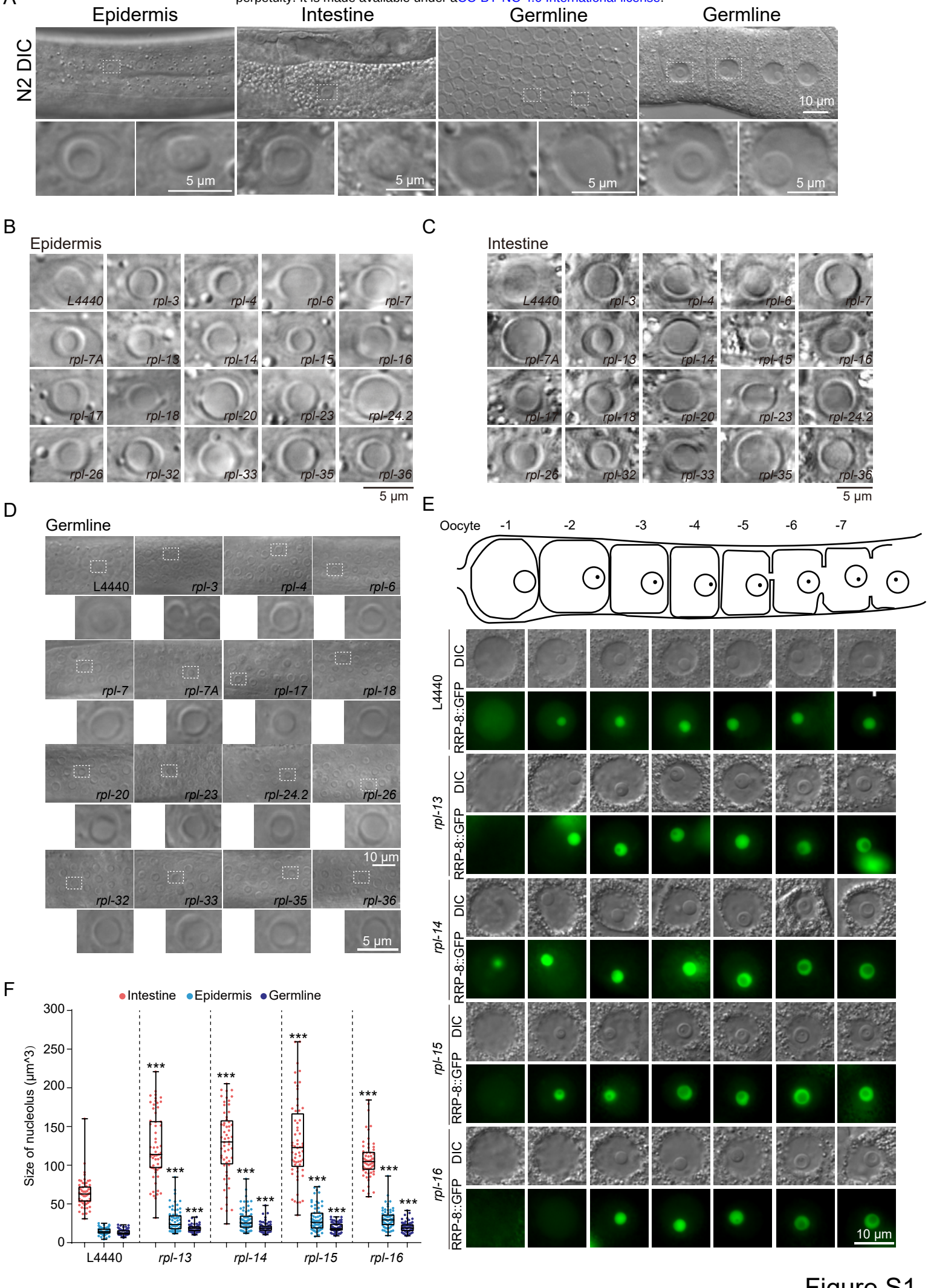

Figure S1

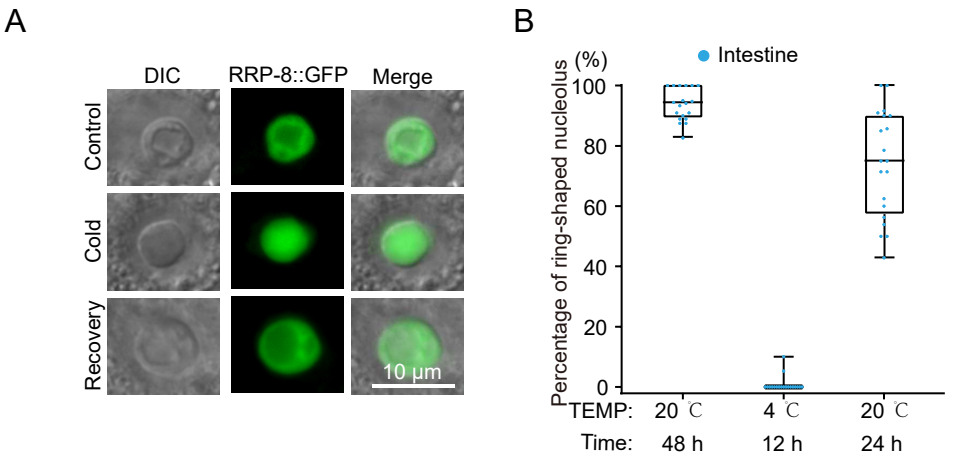

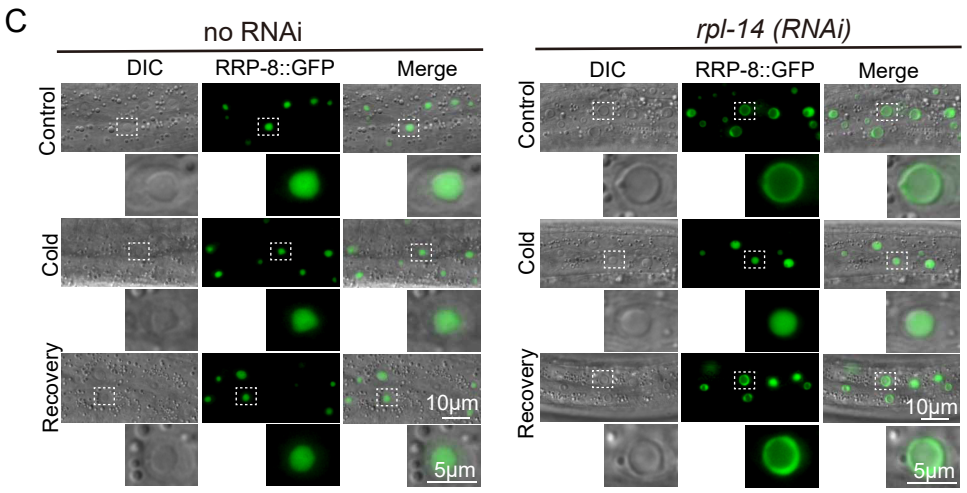

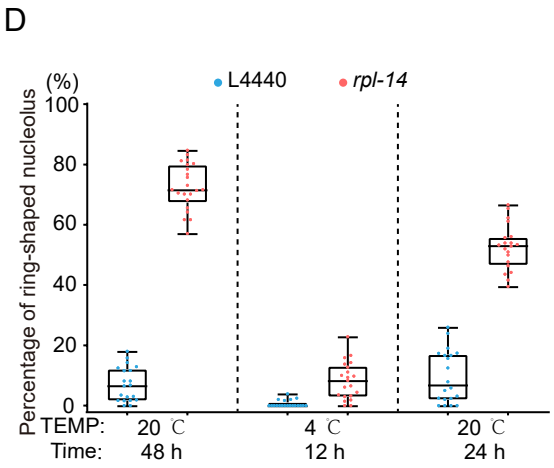

Figure S2

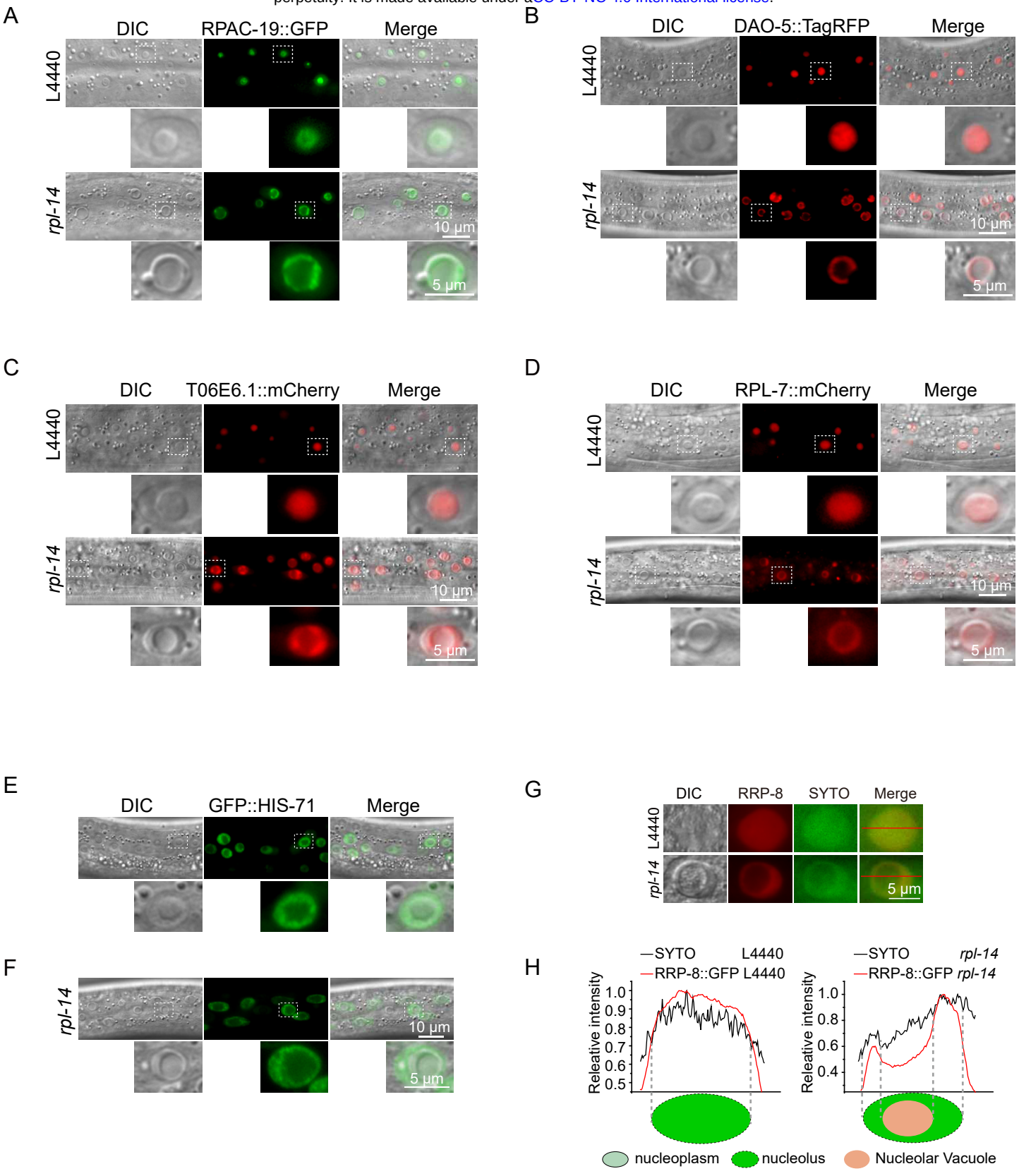

Figure S3

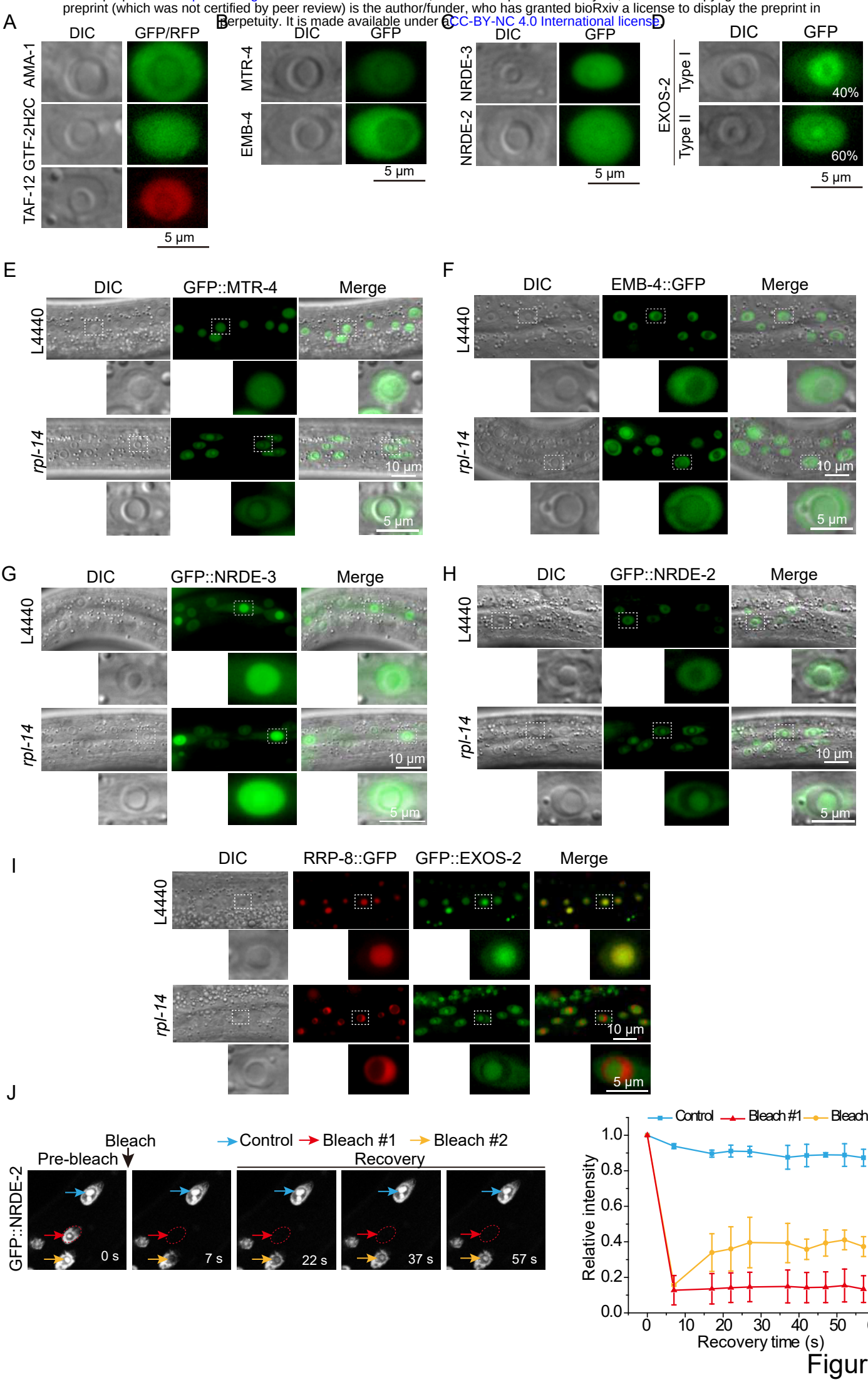

Figure S4

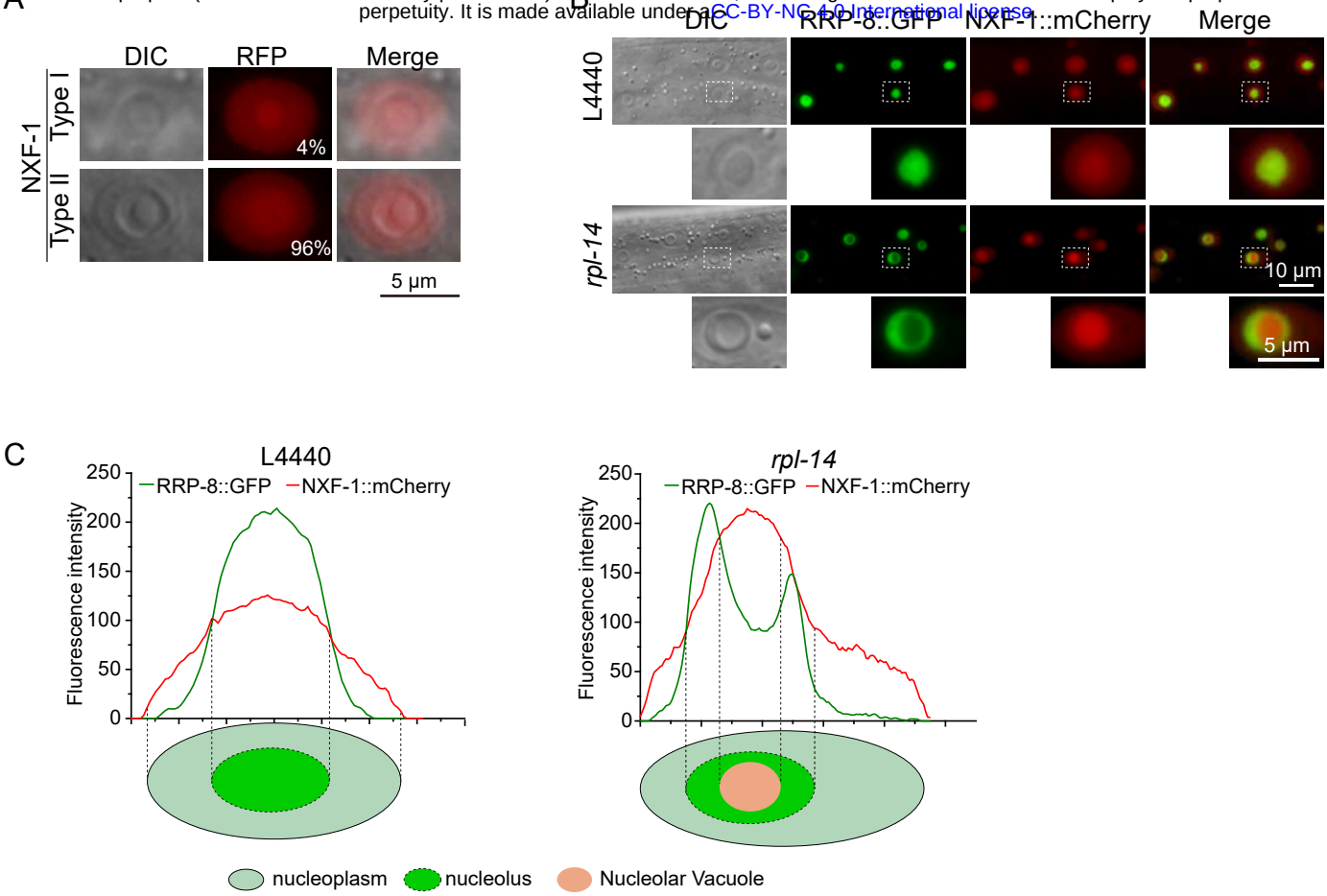

Figure S5

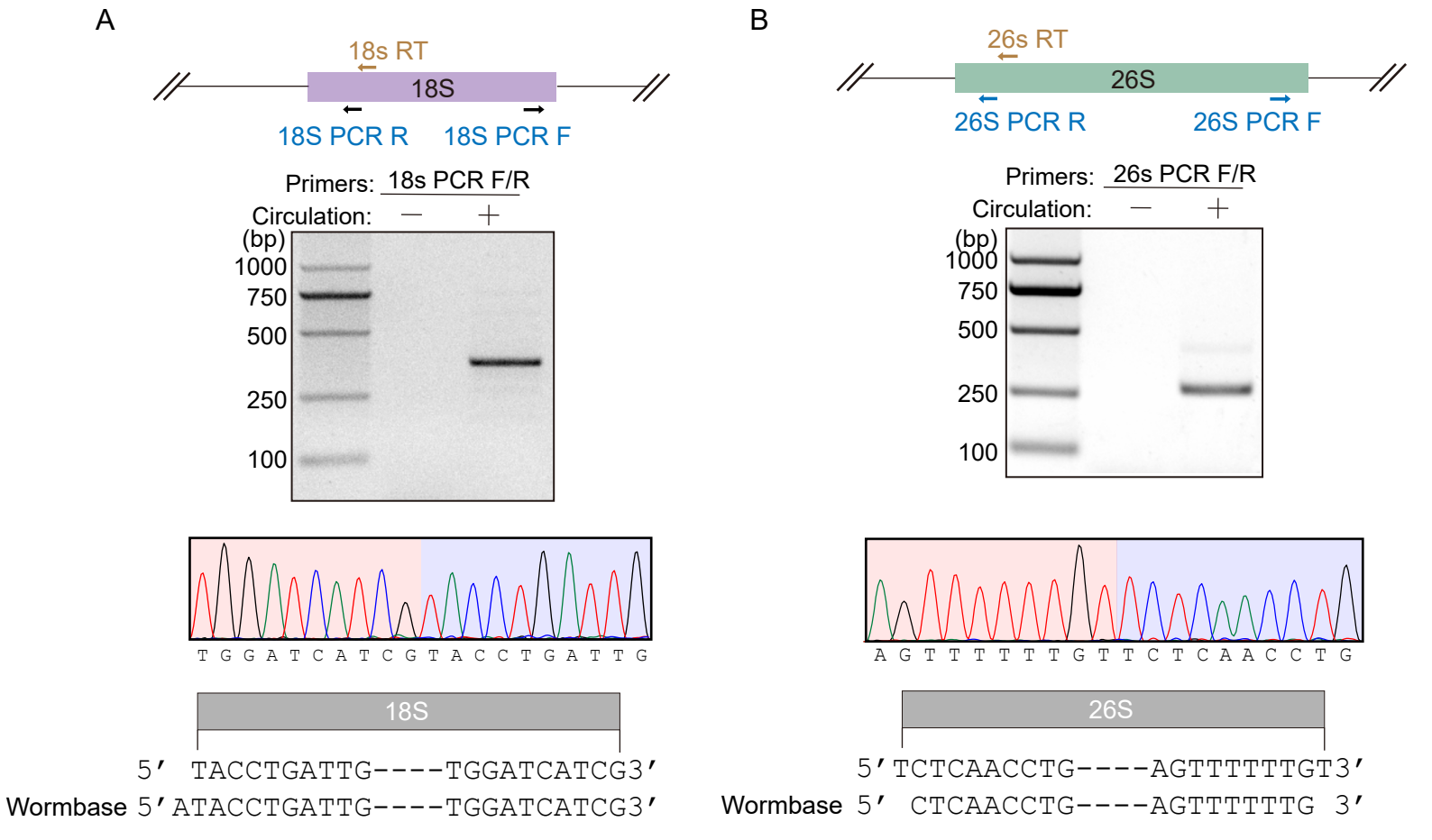

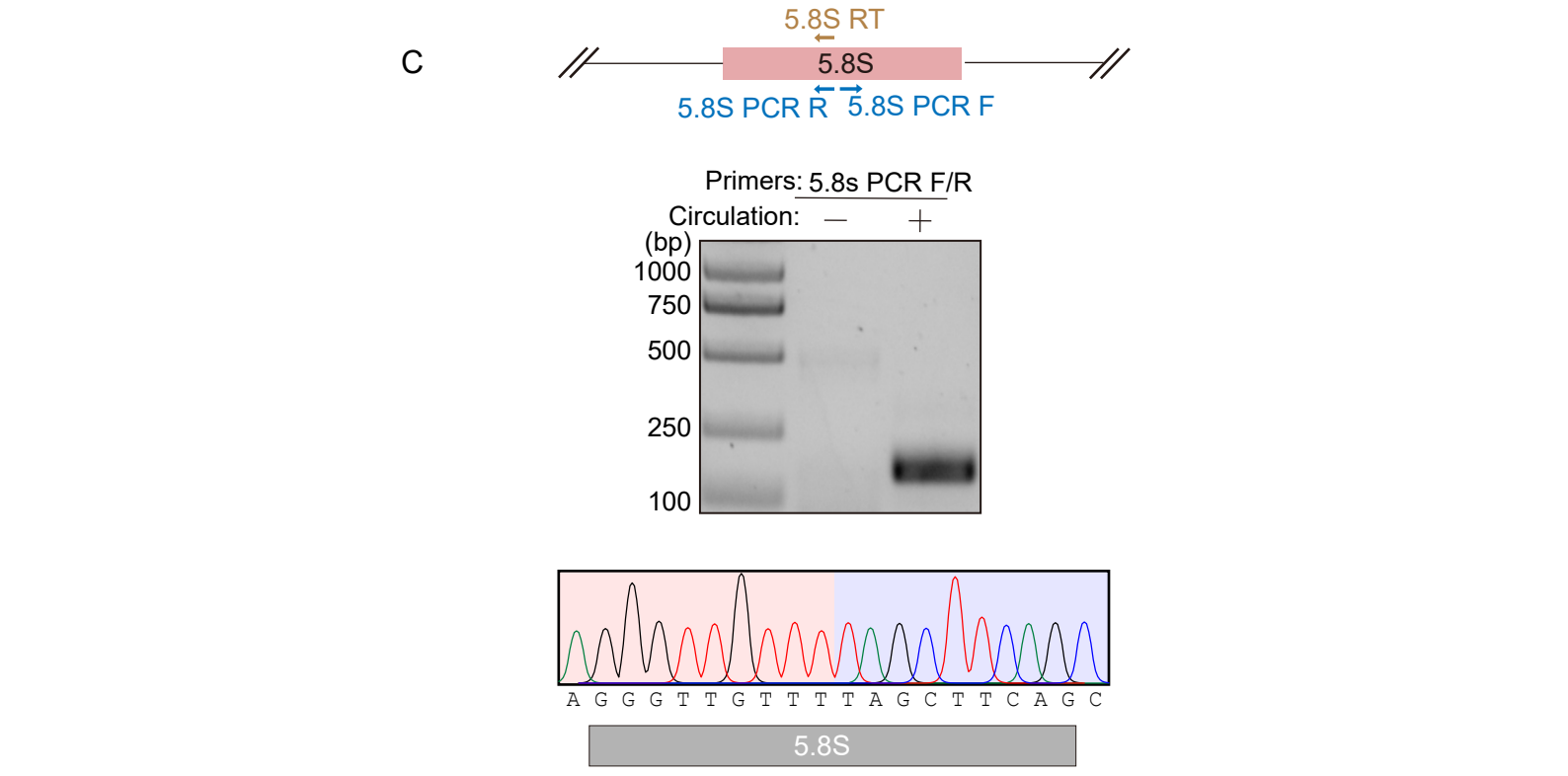

Figure S6

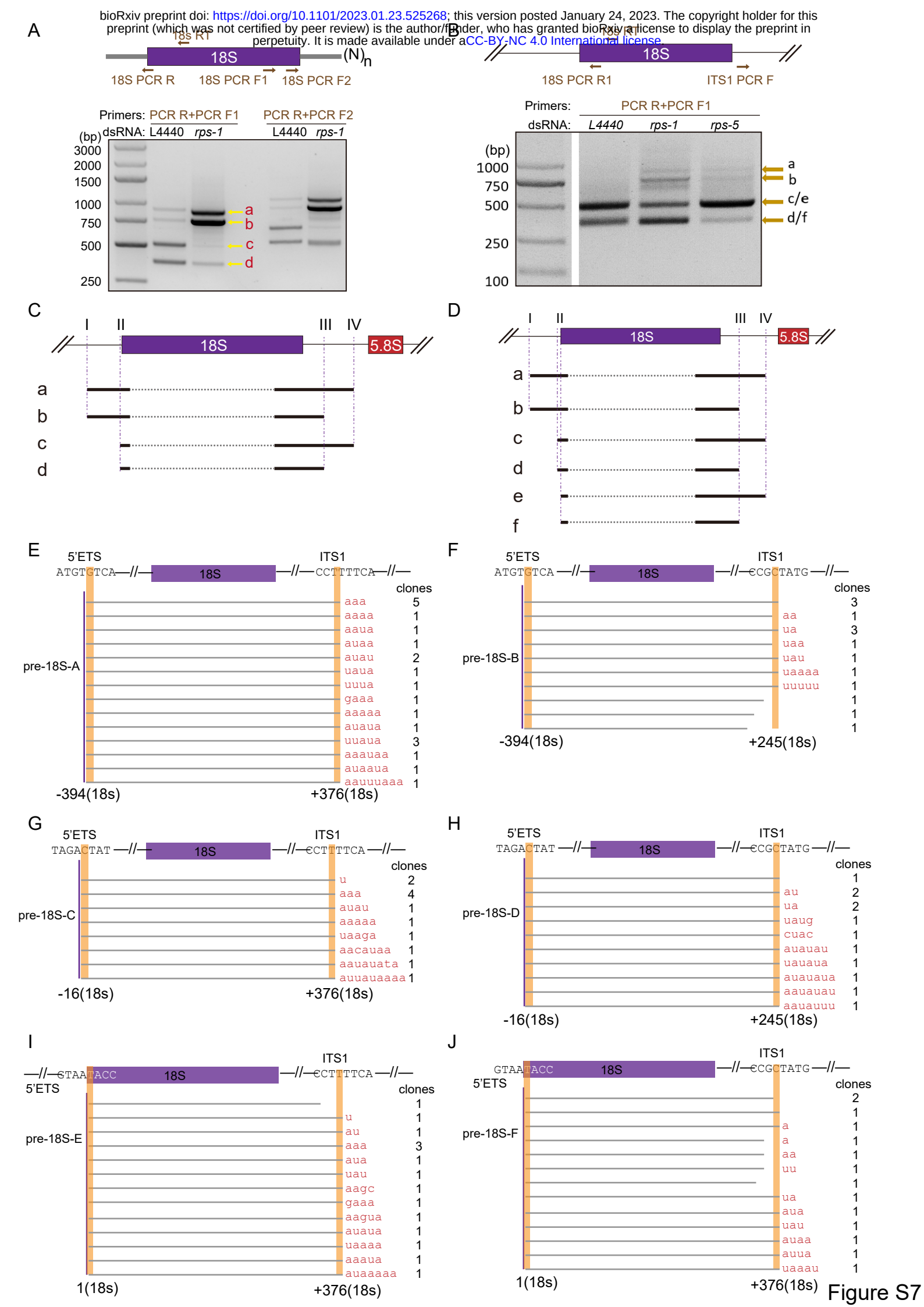

Figure S7

A

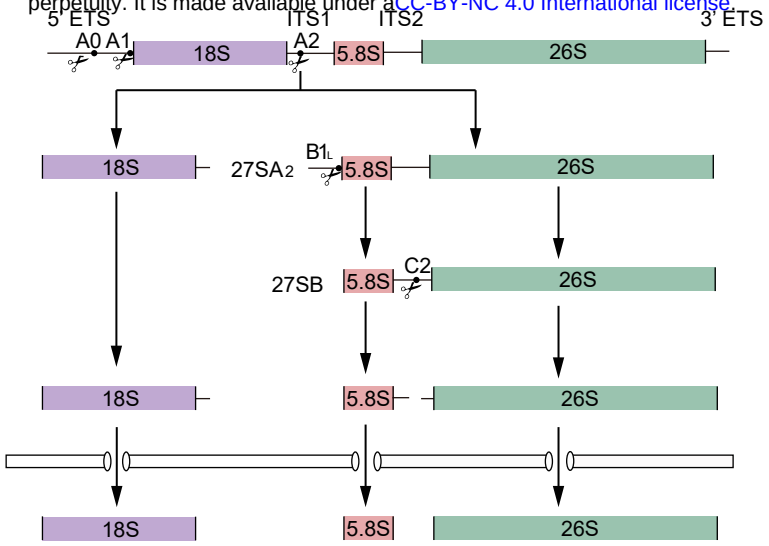

B

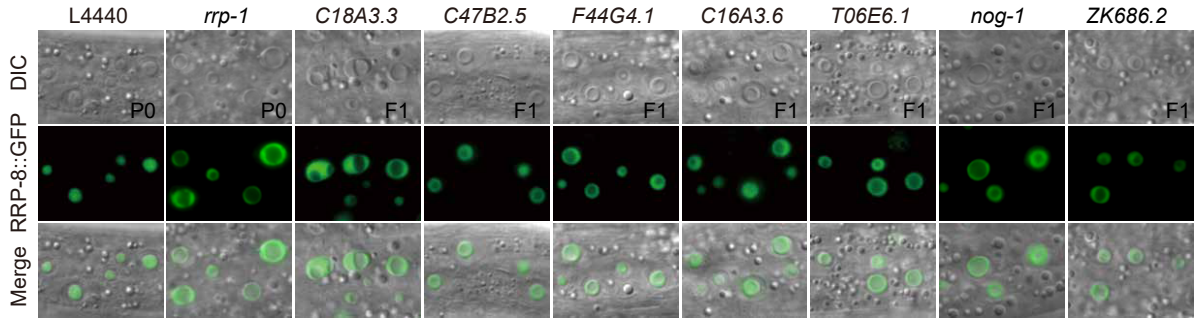

C

Genes	Homlog		Pre-RNA processing	Reference
	H. sapiens	S. cerevisiae		
C18A3.3	EBNA1BP2	EBP2	35S and 27SA↑	HUBER et al. 2000
C47B2.5	EIF6	TIF6	35S and 27SB↑	BASU et al. 2001
F44G4.1	RPF1	RPF1	27SA3↑	HARNPICHARNCHAI et al. 2001
C16A3.6	MAK16	mak16	27SB stability	PELLETT AND TRACY 2006
T06E6.1	WDR74	NSA1	27SA2↑	HIRAISHI et al. 2018
rrp-1	RRP1	RRP1	27SA↑	HORSEY et al. 2004
nog-1	GTPBP4	NOG1	35S↑	KALLSTROM et al. 2003
ZK686.2	DDX51	DBP6	27S↓	KRESSLER et al. 1998

D

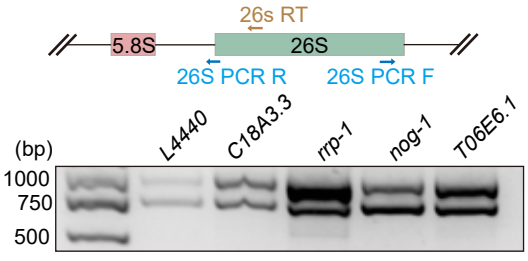

E

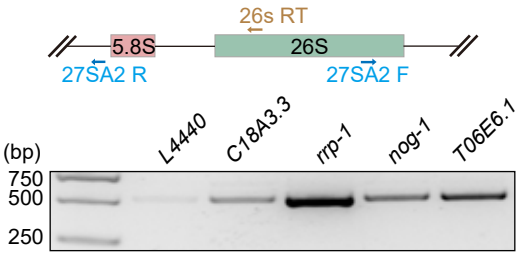

Figure S8

A

Protein	RRM domain	RGG motif	Homolog in human	Funtion
FIB-1	—	+	FBL	nucleologenesis
NUCL-1	+	+	NCL	RNA binding activity
NIFK-1	+	—	NIFK	maturation of LSU-rRNA
RBD-1	+	—	RBM19	rRNA processing
C18A3.3	—	+	EBNA1BP2	rRNA processing
F57B10.8	+	—	ABT1	ribosomal small subunit biogenesis
GARR-1	—	+	GAR1	rRNA pseudouridine synthesis
Y94H6A.5	—	+	DDX54	rRNA processing

B

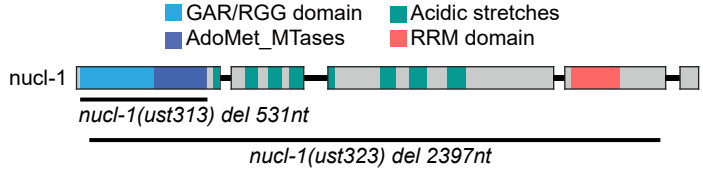

C

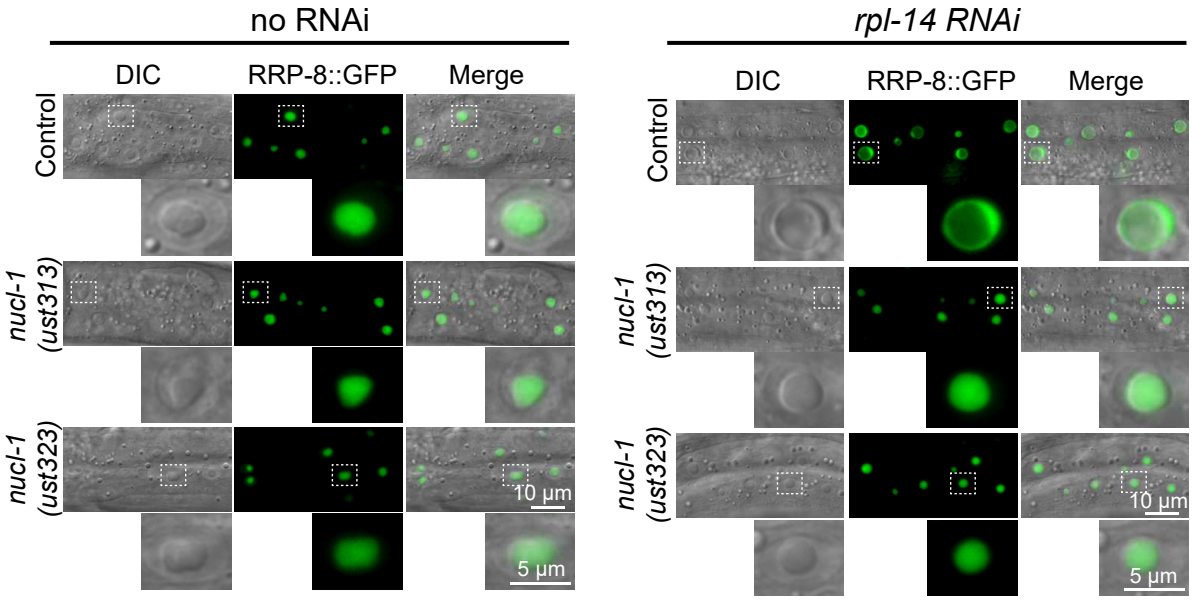

D

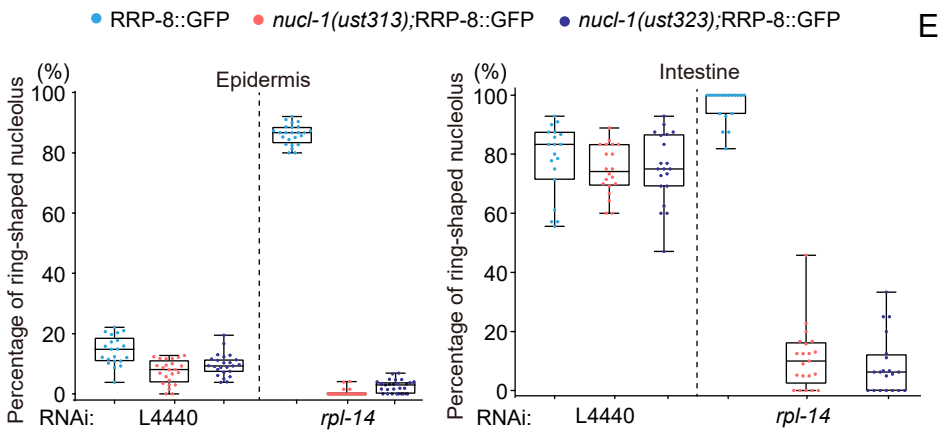

E

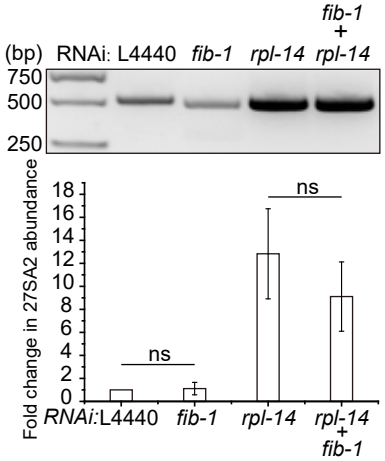

F

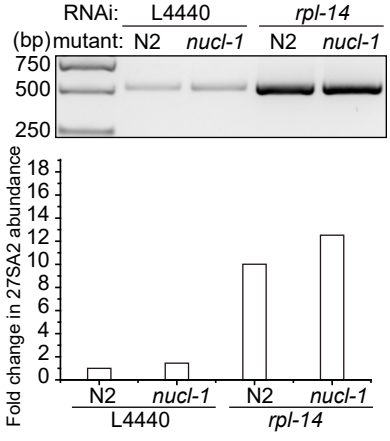

G

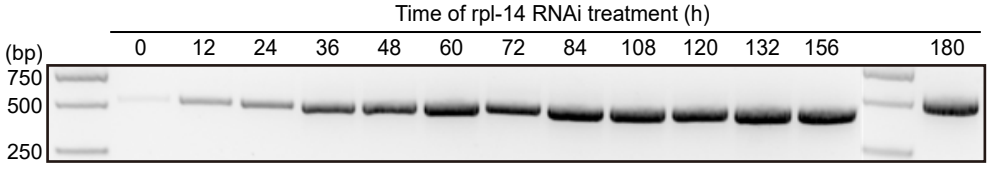

Figure S9

Table S1: Selected rRNA processing and ribosome assembly factors tested by RNAi screening.

Gene ID	Gene ID	Gene ID	Gene ID	Gene ID
Y39A1A.14	F55F8.5	rpl-13	rpl-33	rps-9
F18C5.3	C15H11.9	rpl-14	rpl-34	rps-10
ZK1127.5	W09C5.1	rpl-15	rpl-35	rps-11
T22H9.1	T19A6.2	rpl-16	rpl-36	rps-12
ZC434.4	K01C8.9	rpl-17	rpl-36A	rps-13
T22H6.1	W07E6.2	rpl-18	rpl-37	rps-14
Y54E5B.2	T25G3.3	rpl-19	rpl-38	rps-15
Y75B8A.7	Y56A3A.18	rpl-20	rpl-39	rps-16
C48B6.2	crn-3	rpl-21	rpl-40	rps-17
F58B3.4	rpl-1	rpl-22	rpl-41.1	rps-18
F57B10.8	rpl-2	rpl-23	rpl-41.2	rps-19
ZK430.7	rpl-3	rpl-24.1	rpl-42	rps-20
T20B12.3	rpl-4	rpl-24.2	rpl-43	rps-21
F57B9.5	rpl-5	rpl-25.1	rps-0	rps-22
Y48B6A.3	rpl-6	rpl-25.2	rps-1	rps-23
T01C3.7	rpl-7	rpl-26	rps-2	rps-24
K07C5.4	rpl-7A	rpl-27	rps-3	rps-25
Y6B3B.9	rpl-9	rpl-28	rps-4	rps-26
F54C1.2	rpl-10	rpl-29	rps-5	rps-27
rrp-8	rpl-11.1	rpl-30	rps-6	rps-28
R13A5.12	rpl-11.2	rpl-31	rps-7	rps-29
F23B12.7	rpl-12	rpl-32	rps-8	rps-30

Table S2. List of genes involved in 26S rRNA processing.

Gene ID	Gene ID	Gene ID	Gene ID
rrp-1	C43E11.9	mac-1	F55F8.2
K12H4.3	pro-2	F44G4.1	ddx-15
ddx-17	C37H5.5	ZK546.14	C47B2.5
ZK686.2	T07A9.9	F53E10.6	T06E6.1
C24H12.4	nsun-1	let-716	F23B12.7
C18A3.3	rbm-28	H06I04.3	
C16A3.6	T05H4.10	K09H9.6	

Table S3: List of strains used in this study.

Strains	Genotype
N2	
shg2123	rrp-8::gfp::3xflag (ustIS76)
shg2287	fib-1P::fib-1::mCherry::rps-1 3' UTR (ustIS293)
shg1248	3xflag::gfp::rpoa-2 (ustIS116)
shg2285	rpl-7::mCherry (ustIS291)
shg1092	rrp-8::mCherry (ustIS128)
shg1268	3xflag::gfp::rpoa-1 (ustIS137)
shg1229	3xflag::gfp::rpac-19
shg1889	tagRFP::dao-5 (ustIS242)
shg1660	rbd-1::mCherry (ustIS207)
shg2286	T06E6.1::mCherry (ustIS292)
shg852	3xflag::gfp::nrde-2 (ustIS117)
shg664	mtr-4p::gfp::mtr-4::mtr-4 UTR
shg2288	ama-1::gfp::3xflag (ust423)
YY174	3xflag::gfp::nrde-3 (ggIS1)
shg011	*eri-1(mg366);* ggIS1;susi-1(ust001)
shg1890	3xflag::gfp::his-71 (ustIS254)
shg2160	3xflag::gfp::gtf-2H2C (ust384)
shg1696	taf-12::tagRFP (ustIS227)
shg2289	emb-4::gfp::3xflag (ust424)
shg2141	nxf-1::mCherry (ustIS281)
shg2142	nxf-1::mCherry(ustIS281);rrp-8::gfp(ustIS76)
shg2104	3xflag::gfp::exos-2(ustIS113);rrp-8::mCherry (ustIS128)
shg1914	*nucl-1 (ust313)*
shg2090	*nucl-1 (ust323)*
shg2098	*nucl-1 (ust313);* susi-2::gfp(ustIS76)
shg2143	*nucl-1 (ust323);* susi-2::gfp(ustIS76)

Table S4. Sequences of double-strand RNA for RNAi Screening

Genes	Left Oligo	Right Oligo
rpl-1	GGTAAAATGTCGAAGGTTTC	GTTAATAAACTCTTTGTGGCT
rpl-4	ATGGCGGCCAGACCGCTCGT	ACAGAATACTTATTTCTTCA
rpl-7A	CCTAGCAAGAAGGTTATCAA	TTAGAGCTTTCCAAGATCAC
rpl-9	ATGAAGCTGATCGAGTCTAA	TTAGTCAGTTGGGACGATGG
rpl-12	GATACGGAGTCAATTCGCCG	CAAGTGACAGATCATTGAGC
rpl-15	CATGGGTGCATACAAGTATA	GGTTTGATAACAACCATTTC
rpl-16	ATGGGTCTGTCGAACAGAGC	TTAATTGTATCCAAGAGCCT
rpl-17	GTAATCTTCCTTGTCGAAAT	TTGTGTAACGGGAAACACTT
rpl-18	GGTATTGATATCAACCACAA	CGGCATGATTCGAAAACAAT
rpl-19	CAGCAATCTCCGTCTGCAGA	TTACTTTCCAGCGATAACCT
rpl-21	ATGACTAACTCCAAGGGTCT	TCACGCAACAATCTCGAAAC
rpl-24.1	CAGATTCGTCAAGCGAGGGC	GAACGTTTATCGCTTTCCTC
rpl-26	CAAGCATGTAATTGTCTCTA	ACACTGACGAGACCGTCAAC
rpl-27	ATGGGCAAGATTATGAAGCC	TTAGAATCGCAATTTGGTGA
rpl-28	GTAAAATGTCCGACGCTCTC	CGTGTTGATAAGCTGTAACA
rpl-30	CAGGTAAATCATCATGGCTC	CTGTTTTCAACAATTTATTG
rpl-31	GTAATCCAGTCAAGTCGCGA	CTCGAAAATCAAAACCTTTT
rpl-32	GTAAAATGGTGCACGTTTCC	CGTTTTTCAAAACAAGTTTA
rpl-34	ATGTCCCTCCGCGTTACCTA	GTTTTGCTCGATTAAACTAG
rpl-36	GTAAAATGGTCAACGTGCCA	AACAACATGGTTCTTTATAA
rpl-38	CAGGTAATCCACCATTGCGA	GATAAGACAGGGATGTAACG
rpl-39	CAGGTAATGTCTGCCTTGAA	GAAAATTGAACAACAGATAA
rpl-41.1	CCTTCAATGAATACTGCAAC	CTTAACCAGAATCTTGGACG
rpl-41.2	AACGCTACGCGAATCGATGA	CATTGTAACAGATGGAGTAG
rpl-42	TCGTTAAACTTTACAAATCG	CACAAGTACCATTTATTCAA
fib-1	CTCATACGGCTCCAGGGTTA	TATCGTTTTGATGGCGAACA
nucl-1	TGCAGCTTGAGCGTCTTCTA	CTGGAGTTTTAGCGACAGGC

Table S5. Sequence of repair plasmids primers used in ectopic transgenic strains construction

Strains	Primer name	Sequence
	mCherry-F	GGAGGTGGAGGTGGAGCTATGGTCTCAAAGGGTGAAGAAGA
	mCherry-F	CTTATACAATTCATCCATGC
	vector-F	TATCTGGATCCACGAAGCTT
	vector-R	TCCTGCAGGAATTCCTCGAG
Shg2287	Promoter & CDS-F	CTCGAGGAATTCCTGCAGGAGTCATGAATTCATTTGACAGCTC
Shg2287	Promoter & CDS-R	TAGCTCCACCTCCACCTCCGACCTTCTTTCCCTTGACTGG
Shg2287	UTR-F	GCATGGATGAATTGTATAAGTAAGTCTTATAATTTCATTG
Shg2287	UTR-R	AAGCTTCGTGGATCCAGATACAGGTGGTGCCTCATTCCTT
Shg2285	Promoter & CDS-F	CTCGAGGAATTCCTGCAGGACCCATCTTTACTGCTGAGCTG
Shg2285	Promoter & CDS-R	ATAGCTCCACCTCCACCTCCGACCATTTTTCGGAGAAGGTTGTT
Shg2285	UTR-F	GCATGGATGAATTGTATAAGTAAGTCTTATAATTTCATTG
Shg2285	UTR-R	AAGCTTCGTGGATCCAGATACAGGTGGTGCCTCATTCCTT
Shg2286	Promoter & CDS-F	CTCGAGGAATTCCTGCAGGAGAAGATGGCGACACATGCAAGC
Shg2286	Promoter & CDS-R	ATAGCTCCACCTCCACCTCCAACCCTTTTCTTCTTTTTCAGCAC
Shg2286	UTR-F	GCATGGATGAATTGTATAAGTAGGATATTTTGTTGATTTGTTTCGT
Shg2286	UTR-R	AAGCTTCGTGGATCCAGATACACCAATTGTGTACTTCTCTAGAA

Table S6. Sequence of repair plasmids primers used in in-situ transgenic strains construction

Strains	Primer name	Sequence
	vector-F	CACACGTGCTGGCGTTACCC
	vector-R	TGTGAAATTGTTATCCGCTGG
	3xFLAG::GFP-F	GACTACAAAGACCATGACGG
	3xFLAG::GFP-R	AGCTCCACCTCCACCTCCTTTG
	GFP:: 3xFLAG-F	GGAGGTGGAGGTGGAGCTATGAGTAAAGG
	GFP:: 3xFLAG-R	CTTGTCATCGTCATCCTTGTAATCG
	mCherry-F	GGAGGTGGAGGTGGAGCTATGGTCTCAAAGGGTGAAGAAG
	mCherry-R	GTTGAGCTTGTGCCCGAGC
	tagRFP-F	GGAGGTGGAGGTGGAGCTATGGTGTCCAAGGGAGAAGAACTGA
	tagRFP-R	GTTGAGCTTGTGCCCGAGC
shg1890	left arm-F	GGGTAACGCCAGCACGTGTGCTGCCATTAGATATCAGCCAC
shg1890	left arm-R	CCGTCATGGTCTTTGTAGTCCTTGGTACGAGCCATTTCAATTCTG
shg1890	right arm-F	AAGGAGGTGGAGGTGGAGCTATGGCTCGTACCAAGCAAACC
shg1890	right arm-R	CAGCGGATAACAATTTCACAGTTGATGTTCCTGACAACTGAG
shg2289	left arm-F	GGGTAACGCCAGCACGTGTGCAGGACACACTTCACATGAC
shg2289	left arm-R	ATAGCTCCACCTCCACCTCCTTTCGGTGGTGGCTCTTCAAC
shg2289	right arm-F	ACAAGGATGACGATGACAAGTAGATGGAAAATTCAGCAAATTTGGCCC
shg2289	right arm-R	CAGCGGATAACAATTTCACACAGTGTTGTGTCTGGAAATTTCTG
shg2141	left arm-F	GTTGGGTAACGCCAGCACGTGTGCAATCGCTAAGTTCGTTATGG
shg2141	left arm-R	AGCTCCACCTCCACCTCCATGAGCAAACGCTTCTGCTGGAAC
shg2141	right arm-F	TAAATACTGTTCTATCGACATCTTCAGTATGCTTAGTTCTTC
shg2141	right arm-R	CCAGCGGATAACAATTTCACAGACCATCATTTTCTATATTCC
shg1889	left arm-F	GGGTAACGCCAGCACGTGTGGTTGCGTCCAGATCTTTTAC
shg1889	left arm-R	TCTTCTCCCTTGGACACCATAGCGATCAGGGGTACCCTAA
shg1889	right arm-F	GGAGGTGGAGGTGGAGCTATGAGTTCCGACTTGTATGC
shg1889	right arm-R	CAGCGGATAACAATTTCACAACAACAGGCTTTGGAGTAGG
shg2288	left arm-F	GGGTAACGCCAGCACGTGTGCAGGACACACTTCACATGAC
shg2288	left arm-R	ATAGCTCCACCTCCACCTCCTGAATTTGGATCATAAGTCGGCG
shg2288	right arm-F	ACAAGGATGACGATGACAAGTAAGATTTTTCCCGTTTTTTTGGGC
shg2288	right arm-R	CAGCGGATAACAATTTCACAGCACAAATTACACCGAATGG
shg2160	left arm-F	GGGTAACGCCAGCACGTGTGTCGAGCATCATATGCAGGAA
shg2160	left arm-R	CCGTCATGGTCTTTGTAGTCCTCATCATCATCCATATTTA
shg2160	right arm-F	AAGGAGGTGGAGGTGGAGCTATGGATGATGATGAGCAGAA
shg2160	right arm-R	CAGCGGATAACAATTTCACAGAACATTTCAGCAGACAGTC
shg1696	left arm-F	GGGTAACGCCAGCACGTGTGCGAACTTCTGCATACACTAGTTTTTG
shg1696	left arm-R	ATAGCTCCACCTCCACCTCCAAGTTTCTTGATTTGTTTCTTGAGTAGAG
shg1696	right arm-F	TCGGGCACAAGCTCAACTAAAAATTAATTTTTTTTTGTTTTAATTTTAAT
shg1696	right arm-R	CAGCGGATAACAATTTCACACTCCTCATCAACAACAATATCGG

Table S7. Sequences of sgRNAs for CRISPR/Cas9-mediated gene editing.

name	sequence
his-71 sgRNA#1	CAAGATTCCATATTCACTGG
his-71 sgRNA#2	TTTACTTTCTAATTTTCACA
his-71 sgRNA#3	GGTACGAGCCATTTCAATTC
emb-4 sgRNA#1	TCTTCAACTGCTGGAGCTCC
emb-4 sgRNA#2	GCTGAATTTTCCATCTATTT
emb-4 sgRNA#3	AGAGCCACCACCGAAATAGA
dao-5 sgRNA#1	GTCGGAACTCATAGCGATCA
dao-5 sgRNA#2	GTTGCAGATAACAATCGTGG
dao-5 sgRNA#3	GCGCGTGGTTTGTCGAATGG
ama-1 sgRNA#1	AATTTCAACAATTTTAGAGG
ama-1 sgRNA#2	TATGAATTTGGATCATAAGT
ama-1 sgRNA#3	GGAGAGAAATCTCAAATCAG
gtf-2H2C sgRNA#1	TCAAGGTGAAAAGTATTACT
gtf-2H2C sgRNA#2	ATGAGCAGAAGGGTTACACC
gtf-2H2C sgRNA#3	TAATAAAAGCCACTTCCAGA
taf-12 sgRNA#1	GAAGGAAAAGTTTGTTCCAA
taf-12 sgRNA#2	GCACAATTTTGGGTCTCAAA
taf-12 sgRNA#3	AACGGAAGCACACAAGCAAC
nxf-1 sgRNA#1	TAATGAGCAAACGCTTCTGC
nxf-1 sgRNA#2	TATTTCGTTGAACTTCTGAC
nxf-1 sgRNA#3	AATGTCTTGCAGACTGCGCT
nucl-1 sgRNA#1	GGCAGTGGCTTCACCCCACG
nucl-1 sgRNA#2	CGTTCATCAAGCGGATTCCG
nucl-1 sgRNA#3	GATAGAGGACGTTCTCCAGG
nucl-1 sgRNA#4	AGAGGAAACTTCCAATCTCG
nucl-1 sgRNA#5	GAGGTGGCGTCAAGTGATGA
nucl-1 sgRNA#6	GTCAAGTGATGAAGGAATTC

Table S8. Sequence of cRT-PCR and qPCR primers

Name	Sequence (5' to 3')
5.8s PCR F	AATTGCAGACGCTTAGAGTGG
5.8s RT/5.8s PCR R	CGTGGTAAGTAACGCAGCAAG
26s RT R	CACCTATACGCCACATTTCGAAGC
26s PCR R	GAGTTCAGGTTGAGATTAGCAAGACA
26s PCR F	GGCGTCGTAGTGAATTCTGCG
26s PCR R1	CGTTTCACTCGCCGTTACTAAGG
27SA2-R	CTCAACAACAAATCACCGCATG
27SA2-F	CAGATCAATGGTCTGAAGCTACC
18s RT	GTATAGTTGCATGTATTAGCTCCAG
18S PCR R1	CTGCTCTAATGAGCCGTACGC
18S PCR F1	GGTATTGTAATTATTGCCCTTAAACG
18S PCR F2	GACTTCGTTGTTGCGGAAACC
18s PCR R	CAATCAGGTATTACGCAGACAT
ITS1 PCR F	CATGGAACGTGGCAGTTATTC
27-qRT-F1	GGTGTTGTATTCAGTAGAGCAG
27-qRT-R	CTTTTGGCAATCAGTGTACTGATTC